JGR Atmospheres

RESEARCH ARTICLE
10.1029/2021JD035796

Large Daytime Molecular Chlorine Missing Source at a Suburban Site in East China

Qianjie Chen[1], Men Xia[1], Xiang Peng[1,2], Chuan Yu[1], Peng Sun[3], Yuanyuan Li[3], Yuliang Liu[3], Zhengning Xu[3], Zheng Xu[3], Rongrong Wu[4], Wei Nie[3], Aijun Ding[3], Yu Zhao[4], and Tao Wang[1]

[1]Department of Civil and Environmental Engineering, The Hong Kong Polytechnic University, Hong Kong SAR, China, [2]Department of Ambient Air Quality Monitoring, China National Environmental Monitoring Center, Beijing, China, [3]Joint International Research Laboratory of Atmospheric and Earth System Sciences, School of Atmospheric Sciences, Nanjing University, Nanjing, China, [4]State Key Laboratory of Pollution Control & Resource Reuse and School of the Environment, Nanjing University, Nanjing, China

Key Points:

- Traditional mechanisms underestimate molecular chlorine observations by almost an order of magnitude around noon
- The missing source accounts for about 70% of molecular chlorine production during daytime
- The daytime molecular chlorine missing source could be caused by aerosol photochemistry

Supporting Information:

Supporting Information may be found in the online version of this article.

Correspondence to:

T. Wang and Q. Chen,
tao.wang@polyu.edu.hk;
qianjie.chen@polyu.edu.hk

Citation:

Chen, Q., Xia, M., Peng, X., Yu, C., Sun, P., Li, Y., et al. (2022). Large daytime molecular chlorine missing source at a suburban site in East China. *Journal of Geophysical Research: Atmospheres*, *127*, e2021JD035796. https://doi.org/10.1029/2021JD035796

Received 6 SEP 2021
Accepted 16 JAN 2022

Abstract Molecular chlorine (Cl_2) affects atmospheric oxidative capacity by generating chlorine radicals upon photolysis, but it is poorly simulated in atmospheric chemistry models. In this study, we observed up to 40 ppt Cl_2 around noon at a suburban site in East China, and used a box model with up-to-date chlorine chemistry and comprehensive observational constraints to investigate Cl_2 formation mechanisms. The standard model run with traditional Cl_2 formation mechanisms underestimates the observed Cl_2 by almost one order of magnitude around noon. The daytime Cl_2 missing source was estimated, accounting for on average (69 ± 5)% of daytime Cl_2 production for the 1-week study period. It is likely caused by photochemistry within the aerosols, based on its correlation with observed environmental factors, such as sunlight intensity and aerosol abundances. With the daytime Cl_2 missing source implemented into the model, the chlorine radical abundance increases by a factor of 4 in the afternoon, enhancing the oxidation of volatile organic compounds. A good understanding of daytime Cl_2 formation mechanisms is critical while assessing the impacts of chlorine chemistry on air quality and climate.

Plain Language Summary The photolysis of molecular chlorine gases generates chlorine atoms, which are strong detergent in the lower atmosphere. Chlorine atoms react rapidly with hydrocarbon species in the atmosphere, affecting air quality and climate. High levels of molecular chlorine gases during daytime has been reported recently in China, but it remains unclear how they are formed. In this study, we used a box model to simulate molecular chlorine formation at a suburban site in East China. We propose aerosol photochemistry could be important for molecular chlorine formation during daytime.

1. Introduction

Photolysis of molecular chlorine (Cl_2) generates chlorine radicals (Cl) that react rapidly with hydrocarbons, with implications for methane (CH_4) and dimethyl sulfide (DMS) oxidation, and ozone (O_3) and secondary organic aerosol (SOA) formation in the troposphere (Chen et al., 2018; Hossaini et al., 2016; Qiu et al., 2019; Riva et al., 2015; Simpson et al., 2015; Wang et al., 2019; Wang & Ruiz, 2017). However, the abundance of tropospheric Cl_2 available for daytime photolysis is poorly known, largely due to a lack of observational data and limited understanding of Cl_2 formation mechanisms. Substantial levels of daytime Cl_2 have been sporadically observed in coastal polluted regions (up to 1 ppb; Finley & Saltzman, 2008; Peng, Wang, Wang et al., 2021), inland polluted regions (up to 450 ppt; Liu et al., 2017; Peng, Wang, Xia et al., 2021), and over coastal Arctic snowpack (up to 400 ppt; Liao et al., 2014; McNamara et al., 2019). Other studies have also reported Cl_2* (Cl_2 + HOCl) and nighttime Cl_2 (e.g., Finley & Saltzman, 2006, 2008; Keene et al., 2007; Lawler et al., 2009, 2011; Lee et al., 2010; Pszenny et al., 1993, 2004; Riedel et al., 2012, 2013; Spicer et al., 1998). Large Cl_2 sources are required to sustain high levels of daytime Cl_2 due to its rapid photolysis, which is a challenge for modeling studies using the traditional Cl_2 formation mechanisms (Qiu et al., 2019; Wang et al., 2019). In particular, using the up-to-date gas-phase and multiphase Cl_2 formation mechanisms in the GEOS-Chem global chemical transport model, Wang et al. (2019) were not able to simulate daytime Cl_2 mixing ratios >1 ppt during the WINTER aircraft campaign over the eastern United States, indicating a large daytime Cl_2 source was missing in the model.

Production of Cl_2 occurs via both gas-phase reactions and multiphase reactions on aerosols in the atmosphere. The gas-phase Cl_2 formation pathways, including reaction of $ClONO_2$ with Cl (Equation R1), self-reaction of ClO (Equation R2), and reaction of ClOO with Cl (Equation R3), are very slow and negligible in tropospheric Cl_2 production (Hossaini et al., 2016; Wang et al., 2019). In comparison, the multiphase Cl_2 formation pathways, including uptake of hypochlorous acid (HOCl), chlorine nitrate ($ClONO_2$), nitryl chloride ($ClNO_2$), and hydroxyl radicals (OH) by chloride-containing aerosols (Equations R4–R7), are generally thought to be the dominant sources of Cl_2 in the troposphere (Simpson et al., 2015; Vogt et al., 1996; Wang et al., 2019).

$$ClONO_2 + Cl \rightarrow Cl_2 + NO_3 \quad \text{(R1)}$$

$$ClO + ClO \rightarrow Cl_2 + O_2 \quad \text{(R2)}$$

$$ClOO + Cl \rightarrow Cl_2 + O_2 \quad \text{(R3)}$$

$$HOCl + Cl^- + H^+ \rightarrow Cl_2 + H_2O \quad \text{(R4)}$$

$$ClONO_2 + Cl^- \rightarrow Cl_2 + NO_3^- \quad \text{(R5)}$$

$$ClNO_2 + Cl^- + H^+ \rightarrow Cl_2 + HONO \quad \text{(R6)}$$

$$OH + Cl^-_{surface} \rightarrow 0.5\ Cl_2 + OH^- \quad \text{(R7)}$$

$$Cl_2 + h\nu \rightarrow 2Cl \quad \text{(R8)}$$

Reaction of HOCl with chloride (Cl^-) on acidic aerosols (Equation R4) has been proposed to be an important source of Cl_2 in the marine boundary layer (Lawler et al., 2011; Pechtl & von Glasow, 2007). HOCl is mainly produced from reaction of ClO with HO_2. Pratte and Rossi (2006) measured an uptake coefficient of $(0.4–1.8) \times 10^{-3}$ for HOCl (γ_{HOCl}) onto acidic ($pH \approx -1$) natural sea salt aerosols in their flow tube experiments, but they were not able to determine the γ_{HOCl} onto acidic NaCl aerosols due to detection limit issues. An upper limit of $\gamma_{HOCl} < 2 \times 10^{-4}$ onto acidic ($pH \approx -1$) NaCl aerosols was recommended by the IUPAC Task Group on Atmospheric Chemical Kinetic Data Evaluation (Ammann et al., 2013). Based on ground-based observations of HOCl and Cl_2 in the remote marine boundary layer, Lawler et al. (2011) calculated a γ_{HOCl} of 1.7×10^{-3} to best explain the Cl_2 observations.

Uptake of $ClONO_2$ by aerosols (Equation R5) is especially important for Cl_2 production in the high NO2 environments (McNamara et al., 2019; Wang & Pratt, 2017), as $ClONO_2$ is mainly produced from reaction of ClO with NO_2. The uptake coefficient of $ClONO_2$ (γ_{ClONO2}) on the 0.1 M aqueous NaCl droplets (~200 μm, $pH \approx 6$) was determined in laboratory experiments at 274.6 K to be $(2.44 \pm 0.23) \times 10^{-2}$, very close to that ($(2.41 \pm 0.20) \times 10^{-2}$) on pure water droplets (Deiber et al., 2004). The γ_{ClONO2} is not dependent on temperature, as indicated by the water droplet experiments (Deiber et al., 2004), and the impact of aerosol acidity on γ_{ClONO2} is currently unknown. Release of Cl_2 was observed during uptake of $ClONO_2$ on NaCl droplets (Deiber et al., 2004), consistent with other experiments conducted on solid NaCl (Finlayson-Pitts et al., 1989; Gebel & Finlayson-Pitts, 2001). HOCl was proposed as a product of $ClONO_2$ hydrolysis, but was not observed for both pure water and NaCl droplets, likely due to its high solubility (Deiber et al., 2004). The Henry's law constant of HOCl is about four orders of magnitude higher than that of Cl_2 (Sander, 2015).

Production of Cl_2 from aerosol uptake of $ClNO_2$ (Equation R6) occurs mainly at night, when N_2O_5 reacts with chloride on aerosols to produce $ClNO_2$ (Osthoff et al., 2008; Thornton et al., 2010). In previous laboratory experiments (Roberts et al., 2008), production of Cl_2 was observed when $ClNO_2$ was passed over a deliquesced mixture of NaCl and oxalic acid ($pH \approx 1.8$, $[Cl^-] \approx 0.05$ M), and the $ClNO_2$ uptake coefficient (γ_{ClNO2}) was determined to be $(6 \pm 2) \times 10^{-3}$. In comparison, γ_{ClNO2} on pure water or NaCl solution at neutral pH was measured in another study to be only $(0.3–4.8) \times 10^{-6}$, three orders of magnitude lower (Behnke et al., 1997), suggesting the reaction of $ClNO_2$ and Cl^- is acid-catalyzed (Equation R6). Roberts et al. (2008) suggested a rate coefficient for the $ClNO_2 + Cl^-$ reaction ($k_{ClNO2+Cl-}$) at pH of 1.8 to be $\geq 10^7$ M^{-1} s^{-1}. With such a large rate coefficient, nighttime Cl_2 observations during the WINTER aircraft campaign were significantly overestimated by the GEOS-Chem model (Wang et al., 2019). Furthermore, Haskin et al. (2019) used a box model to calculate the field-derived γ_{ClNO2} during the WINTER aircraft campaign to be only $(2.3 \pm 1.8) \times 10^{-5}$ and a corresponding $k_{ClNO2+Cl-}$ of only

5.7×10^4 M^{-1} s^{-1}. Their low field-derived γ_{ClNO2} and $k_{ClNO2+Cl-}$ suggest that the acid-catalyzed $ClNO_2 + Cl^-$ reaction is volume-limited, with a reacto-diffusive length scale on the order of 15 μm (Haskin et al., 2019).

Uptake of OH radicals by aerosols (Equation R7) can also release Cl_2 into the atmosphere (Knipping & Dabdub, 2002). Several experimental studies have observed Cl_2 production when O_3 and deliquesced sea salt or NaCl particles were irradiated at 254 nm (Knipping et al., 2000; Laskin et al., 2006; Oum et al., 1998). The photolytic Cl_2 source was proposed to be initiated by uptake of O_3-generated OH radicals onto the particle surface, followed by formation and self-reaction of the surface complexes $(OH \cdots Cl^-)_{surface}$ at the gas-liquid interface (Knipping & Dabdub, 2002; Knipping et al., 2000; Laskin et al., 2006). To best fit the experimental data, a parameterization of the OH uptake coefficient (γ_{OH}) was proposed as $\gamma_{OH} = 0.04[Cl^-]$, where $[Cl^-]$ is the aqueous chloride concentration in mol/l (Knipping & Dabdub, 2002). This OH interfacial mechanism was estimated to account for 40% and 20% of Cl radical production in the remote and polluted marine boundary layer, respectively (Knipping & Dabdub, 2002). However, modeling studies suggested this photolytic source was not large enough to explain daytime Cl_2 observations in the polluted rural environment (Qiu et al., 2019) and during the WINTER aircraft campaign (Wang et al., 2019).

Other proposed Cl_2 formation mechanisms, which are especially efficient during daytime, include the photochemistry within aerosols containing both iron(III) and chloride (Equations R9–R14; Lim et al., 2006; Wittmer, Bleicher, Ofner, & Zetzsch, 2015; Wittmer, Bleicher, & Zetzsch, 2015), uptake of O_3 by aerosols (Equation R15; Faxon et al., 2018; Qiu et al., 2019), and titanium dioxide (TiO_2; construction materials) photocatalysis on urban surfaces (Li et al., 2020). These Cl_2 sources are not well understood, and are generally not considered in atmospheric chemistry models. Recently, Qiu et al. (2019) implemented fast O_3 uptake ($\gamma_{O3} = 1 \times 10^{-3}$ during daytime) mechanism into their CMAQ regional model, with uptake of O_3 accounting for more than 80% of Cl_2 production, so that they were able to simulate ~100 ppt of noontime Cl_2 observed at the Wangdu site in North China. Uptake of N_2O_5 by aerosols, followed by reactions involving NO_2^+ and Cl^-, could be an important Cl_2 source at night (Xia et al., 2020). In addition, Cl_2 can be emitted from anthropogenic activities directly (e.g., industrial processes, power generation, and waste water treatment; Riedel et al., 2012, 2013; Yi et al., 2021) and ground snowpack in polar regions (Liao et al., 2014; Wang & Pratt, 2017).

$$FeCl^{2+} + h\nu \rightarrow Fe^{2+} + Cl_{(aq)} \quad \text{(R9)}$$

$$FeCl_2^+ + h\nu \rightarrow FeCl^+ + Cl_{(aq)} \quad \text{(R10)}$$

$$Cl_{(aq)} + Cl^- \rightleftharpoons Cl_2^- \quad \text{(R11)}$$

$$Cl_{(aq)} + Cl_2^- \rightleftharpoons Cl^- + Cl_2 \quad \text{(R12)}$$

$$Cl_2^- + Cl_2^- \rightarrow Cl_3^- + Cl^- \quad \text{(R13)}$$

$$Cl_3^- \rightleftharpoons Cl_2 + Cl^- \quad \text{(R14)}$$

$$O_3 + 2Cl^- \xrightarrow{H_2O} Cl_2 + 2\ OH^- + O_2 \quad \text{(R15)}$$

Hitherto, very few modeling studies have been conducted to simulate daytime Cl_2 formation and compare with Cl_2 observations in the field (Qiu et al., 2019; Wang et al., 2019; Wang & Pratt, 2017). Recent modeling studies showed that the traditional Cl_2 formation mechanisms (Equations R1–R7) were not able to reproduce high levels of daytime Cl_2 observed in eastern United States (Wang et al., 2019) and North China Plain (Qiu et al., 2019), suggesting an underestimate of chlorine chemistry impacts on atmospheric oxidative capacity. In this study, we investigate daytime Cl_2 formation mechanisms that contribute to the elevated levels of Cl_2 (>10 ppt around noon) observed at a suburban site in East China (Section 3.1). We simulated chlorine chemistry using a box model (Section 3.2), and calculated the daytime Cl_2 missing source that cannot be explained by traditional Cl_2 formation mechanisms. Furthermore, the correlation between this daytime Cl_2 missing source and different environmental factors were analyzed, and potential causes were discussed (Section 3.3). The impacts of this daytime Cl_2 missing source on atmospheric oxidative capacity were also discussed (Section 3.4).

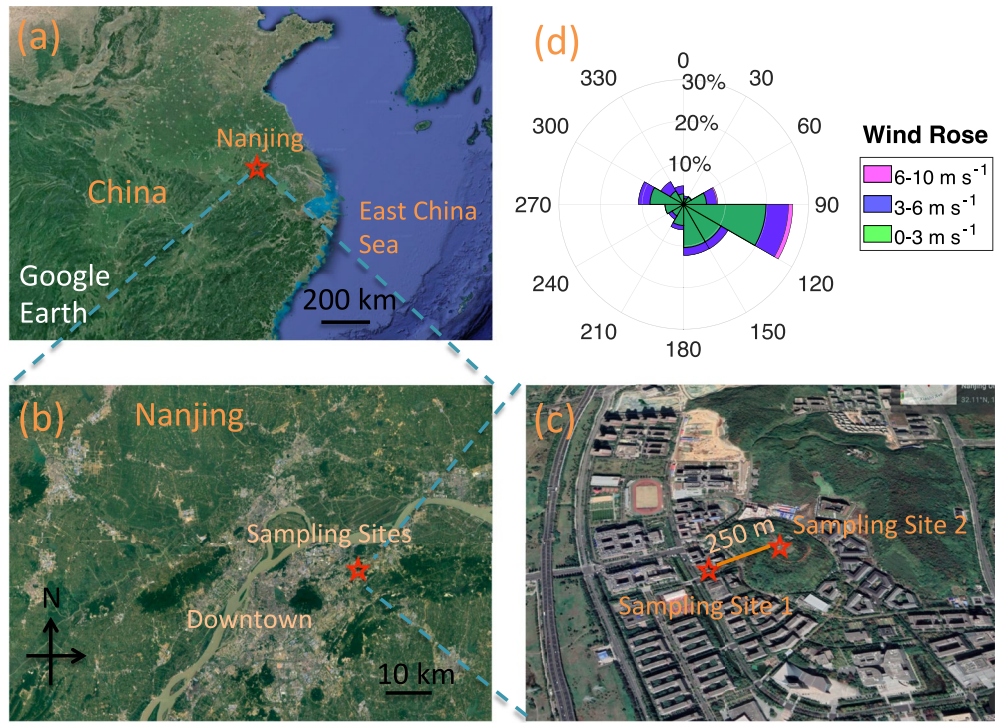

Figure 1. The sampling site information: (a) Location of Nanjing city in China. (b) Location of the sampling sites in Nanjing. (c) Location of sampling site 1 (School of Atmospheric Sciences) and sampling site 2 (SORPES station) in the Xianlin Campus of Nanjing University. (d) The wind rose (percentage distribution of wind speed and direction) measured at 9 m at the SORPES station.

2. Methods and Data

2.1. Measurements Conducted at the Nanjing Suburban Site

During 13–20 April 2018, we conducted measurements of trace gases, aerosols, and meteorological parameters at the Xianlin Campus of Nanjing University (32.12°N, 118.95°E), which is located in a suburban area about 20 km northeast of downtown Nanjing, China (Figures 1a–1c; Ding et al., 2019; Xia et al., 2020). The main land cover types were teaching and residential buildings, vegetation, and sparse roads within 1–2 km of our sampling sites. Significant local emissions of nitrogen oxides (NO_x) and chlorine species were not expected. At about 15 km northwest of the sampling sites, there were chemical and steel facilities (Xia et al., 2020; Zhou et al., 2017) that could emit NO_x, sulfur dioxide (SO_2), carbon monoxide (CO), volatile organic compounds (VOCs), and aerosol particles into the atmosphere. The wind speed measured at 9 m at the SORPES station was rather low during the study period (83% of period below 3 m s^{-1}, on average 2.6 ± 1.4 m s^{-1} during daytime and 2.0 ± 1.0 m s^{-1} during nighttime; Figure 1d). The wind was mainly (77%) from the east while downtown Nanjing and industrial regions were in the west (Figure 1d).

The measurements of Cl_2, $ClNO_2$, dinitrogen pentoxide (N_2O_5), O_3, nitrogen dioxide (NO_2), nitric oxide (NO), and some VOCs species (by gas chromatography; Wu et al., 2020) were made at the fifth floor (~15 m elevation) of building of School of Atmospheric Sciences (SAS) at the Xianlin Campus (sampling site 1, Figure 1c). In particular, Cl_2 and $ClNO_2$ were measured with the PolyU iodide-adduct quadrupole chemical ionization mass spectrometer (Q-CIMS, THS Instruments, Marietta, GA, USA), with detection limits of 5 and 2 ppt and uncertainties of 15% and 19%, respectively (Xia et al., 2020). The daytime Cl_2 dataset has not been analyzed in Xia et al. (2020). The isotopic signals of $ClNO_2$ and Cl_2 are shown in Figure S9 in Supporting Information S1. The isotopic ratio (*m/z* 210 vs. *m/z* 208) of the ambient $ClNO_2$ signals (0.315) is in good agreement with the natural abundance (0.32; Figure S9a in Supporting Information S1). However, there is discrepancy between the ambient Cl_2 isotopic ratio (*m/z* 199 vs. *m/z* 197; 0.558) and the natural abundance (0.64; Figure S9c in Supporting Information S1), indicating there could be unknown interference of the Cl_2 measurements. Our ambient Cl_2

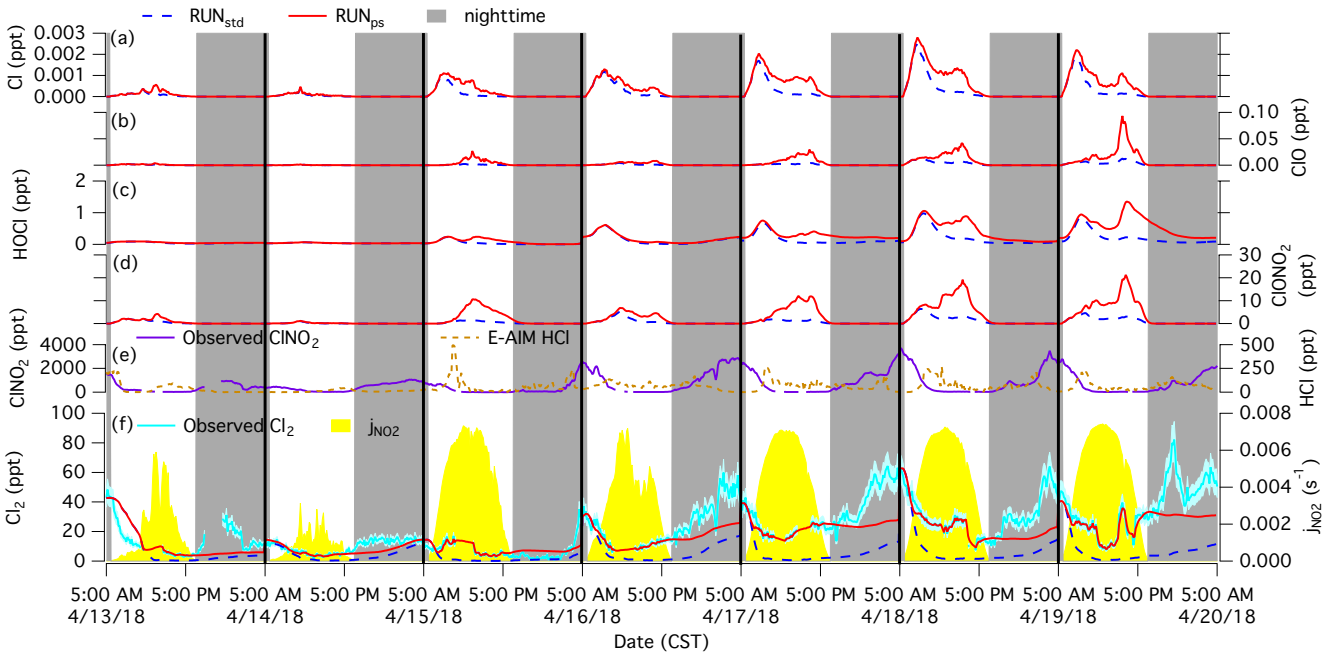

Figure 2. Modeled and observed chlorine species abundances at the Nanjing (China) suburban site from April 13 to 20, 2018. The modeled (a) Cl, (b) ClO, (c) HOCl, (d) $ClONO_2$, and (f) Cl_2 mixing ratios in both the standard model run (RUN_{std}) and the prescribed-source run (RUN_{ps}) are shown. Each case day simulation starts at 05:00 a.m. The (f) observed Cl_2 (±15% uncertainties) and (e) observed $ClNO_2$ and E-AIM modeled HCl (HCl/Cl^- thermodynamic equilibrium) are also shown. The NO_2 photolysis frequency is shown in yellow shading and the nighttime periods are shown in gray shading.

isotopic ratio is close to that (0.58) observed in a previous field study at a rural site on the North China Plain (Liu et al., 2017). The observed Cl_2 is unlikely a result of HOCl, $ClONO_2$, and $ClNO_2$ conversion in the sampling inlet. The HOCl mixing ratio calculated from the model is <2 ppt. With the upper limit of conversion fraction (15%) in a previous study (Liao et al., 2014), it will contribute <0.3 ppt of Cl_2 through inlet conversion. If the observed Cl_2 signals were caused by HOCl or $ClONO_2$ inlet conversion, one would expect a noontime peak of Cl_2 as HOCl and $ClONO_2$ are mainly produced during daytime, but observed Cl_2 showed a nighttime peak (Figure 2). From our sampling inlet wall loss test, Cl_2 formation from $ClNO_2$ conversion in the inlet is negligible (Xia et al., 2020). If the observed Cl_2 signals were caused by $ClNO_2$ inlet conversion, one would expect nighttime Cl_2 to be ~20 times higher than Cl_2 around noon as $ClNO_2$ is on average 1,000 ± 845 ppt at night and only 52 ± 46 ppt around noon, but the diel variation of Cl_2 is not that large (<3 times; Figure 2).

Other measurements were made at the SORPES station (Ding et al., 2019) on a small hill (~40 m elevation; sampling site 2, Figure 1c) about 250 m northeast of the sampling site 1, including nitrous acid (HONO), ammonia (NH_3), SO_2, CO, aerosol chemical composition and size distribution, temperature (T), relative humidity (RH), wind speed and direction, NO_2 photolysis frequency (j_{NO2}), and other VOCs species (by proton transfer reaction-mass spectrometry; Xu et al., 2021). The O_3 mixing ratios measured at the sampling site 1 and sampling site 2 match very well with each other (Figure S13 in Supporting Information S1). The measurements of VOCs by gas chromatography (GC 580, PE; Wu et al., 2020) and proton transfer reaction-mass spectrometry (PTR-MS, Ionicon Analytik; Innsbruck, Austria; Xu et al., 2021) cover major alkanes (e.g., ethane and propane), alkenes (e.g., ethylene and propylene), aromatics (e.g., benzene and toluene), aldehydes (e.g., formaldehyde and acetaldehyde), alcohols (e.g., methanol and ethanol), and organic acids (e.g., formic acid and acetic acid) that react with Cl radicals (see Supporting Information). The average values of the measured VOCs species are shown in Table S1 in Supporting Information S1. More details about the measurement station and instruments could be found from Ding et al. (2016, 2019) and Xia et al. (2020).

2.2. Box Modeling

The box model used in this study is the Framework for 0D Atmospheric Modeling (F0AM) version 4.0.2 (Wolfe et al., 2016; https://github.com/AirChem/F0AM). The Master Chemical Mechanism (MCM) version 3.3.1 was

Table 1
Heterogeneous Cl_2 Formation Mechanisms Added in the F0AM Box Model

ID	Reactions	Reactive uptake coefficient (γ)	References
TD1	$ClONO_2 + Cl^- \rightarrow Cl_2 + NO_3^-$	$\gamma_{ClONO2} = 2.4 \times 10^{-2}$	Deiber et al. (2004)
TD2	$HOCl + Cl^- + H^+ \rightarrow Cl_2 + H_2O$	$\frac{1}{\gamma_{HOCl}} = \frac{1}{\gamma_d} + \frac{1}{\alpha_b} + \frac{1}{\Gamma_b}$; $\Gamma_b = 4H_{HOCl}RT\sqrt{D_l k_{HOCl}[Cl^-][H^+]}f_r/c$ $f_r = \coth(r/l_r) - l_r/r$; $l_r = \sqrt{D_l k_{HOCl}[Cl^-][H^+]}$ $k_{HOCl} = 1.5 \times 10^4\ M^{-2}\ s^{-1}$; $D_l = 2 \times 10^{-5}\ cm^2\ s^{-1}$; $\alpha_b = 0.8$	Wang et al. (2019)
TD3	$ClNO_2 + Cl^- + H^+ \rightarrow Cl_2 + HONO$	$\frac{1}{\gamma_{ClNO2}} = \frac{1}{\gamma_d} + \frac{1}{\alpha_b} + \frac{1}{\Gamma_b}$; $\Gamma_b = 4H_{ClNO2}RT\sqrt{D_l k_{ClNO2}[Cl^-]}f_r/c$; $f_r = \coth(r/l_r) - l_r/r$; $l_r = \sqrt{D_l k_{ClNO2}[Cl^-]}$ $k_{ClNO2} = 5.7 \times 10^4\ M^{-1}\ s^{-1}$; $D_l = 1 \times 10^{-5}\ cm^2\ s^{-1}$; $\alpha_b = 0.01$	Wang et al. (2019); Haskin et al. (2019)
TD4	$OH + Cl^- \rightarrow 0.5Cl_2 + OH^-$	$\gamma_{OH} = 0.04[Cl^-]$	Knipping and Dabdub (2002)
SEN5	$O_3 + 2Cl^- \xrightarrow{H_2O} Cl_2 + 2\ OH^- + O_2$	$\gamma_{O3} = 1 \times 10^{-5}$–$1 \times 10^{-3}$	Faxon et al. (2018)

Note. Reactions TD1, TD2, TD3, and TD4 are included in the standard model run (RUNstd), whereas reaction SEN5 is included in a sensitivity run (RUN_{O3}).

used to simulate gas-phase chemistry (http://mcm.leeds.ac.uk/MCM/). The gas-phase chlorine chemistry follows Xue et al. (2015) and Wang et al. (2019), with Cl reacting with a comprehensive list of VOCs added to the F0AM box model (Tables S2 and S3 in Supporting Information S1). Heterogeneous Cl_2 formation mechanisms from uptake of $ClONO_2$, $ClNO_2$, HOCl, and OH by aerosols (Equations R4–R7) were implemented into the model (Table 1), following the first-order loss approach (Ammann et al., 2013):

$$\frac{d[X]}{dt} = -\frac{c\gamma}{4}S[X] \quad \text{(E1)}$$

where X represents HOCl, $ClONO_2$, $ClNO_2$, or OH; c is the mean thermal velocity of X (unit: cm s^{-1}), S is the aerosol surface area concentration (unit: $cm^2\ cm^{-3}$), and γ (unitless) is the reactive uptake coefficient of X. γ_{ClONO2} was taken as 2.4×10^{-2}, following Deiber et al. (2004). γ_{OH} was parameterized as $\gamma_{OH} = 0.04[Cl^-]$, following Knipping and Dabdub (2002). γ_{HOCl} and γ_{ClNO2} were calculated explicitly by considering gas diffusion, mass accommodation, and chemical reactions in the aerosols (Equations E2–E6), following Wang et al. (2019) and Haskin et al. (2019).

$$\frac{1}{\gamma_Y} = \frac{1}{\gamma_d} + \frac{1}{\alpha_b} + \frac{1}{\Gamma_b} \quad \text{(E2)}$$

$$\gamma_d = \frac{4D_g}{cr} \quad \text{(E3)}$$

$$c = \sqrt{\frac{8R_{SI}T}{\pi M_Y}} \quad \text{(E4)}$$

$$D_g = \frac{3\sqrt{R_{SI}T\left(1/M_r + 1/M_{air}\right)/2\pi}}{8\rho_{air}\sigma^2} \quad \text{(E5)}$$

$$\Gamma_{b,HOCl} = 4H_{HOCl}RT\sqrt{D_l k_{HOCl}[Cl^-][H^+]}f_r/c \quad \text{(E6i)}$$

$$\Gamma_{b,ClNO2} = 4H_{ClNO2}RT\sqrt{D_l k_{ClNO2}[Cl^-]}f_r/c \quad \text{(E6ii)}$$

where Y represents HOCl or $ClNO_2$; γ_d, α_b (0.8 for HOCl and 0.01 for $ClNO_2$; Wang et al., 2019), and Γ_b are gas-phase diffusion coefficients, mass accommodation coefficients and bulk reaction coefficients for HOCl or $ClNO_2$, respectively; D_g is the gas phase diffusion coefficient of HOCl or $ClNO_2$, calculated as a function of air temperature (T) and air density (ρ_{air}); c is the average thermal velocity of HOCl or $ClNO_2$; r is the aerosol particle radius measured; M_{HOCl} (52.5 g mol^{-1}), M_{ClNO2} (81.5 g mol^{-1}), and M_{air} (29 g mol^{-1}) are the molar mass of HOCl, $ClNO_2$, and air, respectively; R_{SI} (8.31 J K^{-1} mol^{-1}) is the universal gas constant; H_{HOCl} (650 M atm^{-1}) and H_{ClNO2} (0.024 M atm^{-1}) are the Henry's law constants of HOCl and $ClNO_2$, respectively (Sander, 2015); D_l is the liquid phase diffusion coefficient for HOCl (2×10^{-5} cm^2 s^{-1}) or $ClNO_2$ (1×10^{-5} cm^2 s^{-1}; Wang et al., 2019); k_{HOCl} (1.5×10^4 M^{-2} s^{-1}; Wang et al., 2019) and k_{ClNO2} (5.7×10^4 M^{-1} s^{-1}; Haskin et al., 2019) are the reaction rate coefficients for HOCl and $ClNO_2$ with Cl^-, respectively; f_r (=coth(r/l_r) − l_r/r) is the spherical correction to mass transfer that compares the reacto-diffusive length scale l_r ($\sqrt{D_l k_{HOCl}[Cl^-][H^+]}$ for HOCl and $\sqrt{D_l k_{ClNO2}[Cl^-]}$ for $ClNO_2$) with aerosol particle radius. The aerosol liquid water content and acidity were obtained from the E-AIM thermodynamics model (Models IV and III; www.aim.env.uea.ac.uk/aim/aim.php). The E-AIM model IV is only applicable when relative humidity is above 60%, covering 53% of the study period. The E-AIM model III (at 298.15 K) was used for the rest period, with an average air temperature of 293 ± 5 K. HCl/Cl^- acid displacement thermodynamics was also considered with the E-AIM model. The distributions of γ_{HOCl} and γ_{ClNO2} at different particle size are shown in Figure S11 in Supporting Information S1.

The integration time for each model step is 10 min. Physical processes, such as dilution, advection, and deposition were not explicitly accounted for in the box model in this study. Instead, a first-order physical loss process with a lifetime of 24 hr for all species was included in the model to represent dilution/advection/deposition, following previous F0AM box modeling studies (e.g., Baier et al., 2017; Kim et al., 2013; Lee et al., 2021; Wolfe et al., 2014, 2016). The inclusion of this 24-hr-lifetime physical loss process in the model has negligible influence on the modeled daytime Cl_2 mixing ratios and missing sources (Table S4 in Supporting Information S1), mainly because the daytime chlorine chemistry is typically fast (e.g., ~10 min for Cl_2 lifetime around noon) and we have a lot of observational constraints in the model, including for example, O_3, NO_x, $ClNO_2$, N_2O_5, HONO, and VOCs. The "HYBRID" method within F0AM (Wolfe et al., 2016), based on TUV v5.2 solar spectra, was used to calculate the photolysis frequencies for all the species. The modeled j_{NO2} was compared to the observed j_{NO2} to get the correction factor (j_{corr} = observed/modeled) every 10 min. Then j_{corr} was applied to all the species to correct for photolysis frequencies. Note that this is a rough approach to allow the model to consider influence of attenuated radiation (e.g., by clouds and aerosols) on photolysis rates and does not account for spectral dependence. The absorption cross sections and quantum yields for NO_2 and Cl_2 are shown in Figure S10 in Supporting Information S1, with unity quantum yields for both species at the 300–400 nm wavelength. Observations of NO_2, NO, O_3, CO, $ClNO_2$, HCl (E-AIM predicted), HONO, N_2O_5, and a series of VOC species measured by PTR-MS (Table S1 in Supporting Information S1; C_5H_8, BENZENE, TOLUENE, STYRENE, HCHO, CH_3CHO, CH_3OH, C_2H_5OH, HCOOH, CH_3COOH, BENZAL, CRESOL, MEK, DMS, HEXANAL, and PHENOL) were used to constrain the model every 10 min. CH_4, H_2, and other VOC species measured by GC-MS (Table S1 in Supporting Information S1; C_2H_4, C_2H_6, C_3H_6, C_3H_8, NC_4H_{10}, IC_4H_{10}, NC_5H_{12}, IC_5H_{12}, NC_6H_{14}, EBENZ, MXYL, OXYL, and PXYL) were fixed in the model with values listed in Table S1 in Supporting Information S1.

The standard model simulations (RUN_{std}) include uptake of $ClONO_2$, $ClNO_2$, HOCl, and OH by aerosols (Table 1, TD1–TD4). Each case day, that is, (a) April 13 05:00–April 14 05:00, (b) April 14 05:00–April 15 05:00, (c) April 15 05:00–April 16 05:00, (d) April 16 05:00–April 17 05:00, (e) April 17 05:00–April 18 05:00, (f) April 18 05:00–April 19 05:00, and (g) April 19 05:00–April 20 05:00, was simulated separately, starting at 05:00 a.m. in order to better capture the daytime variability of Cl_2. For each case day, we spun up the model for 48 hr, upon

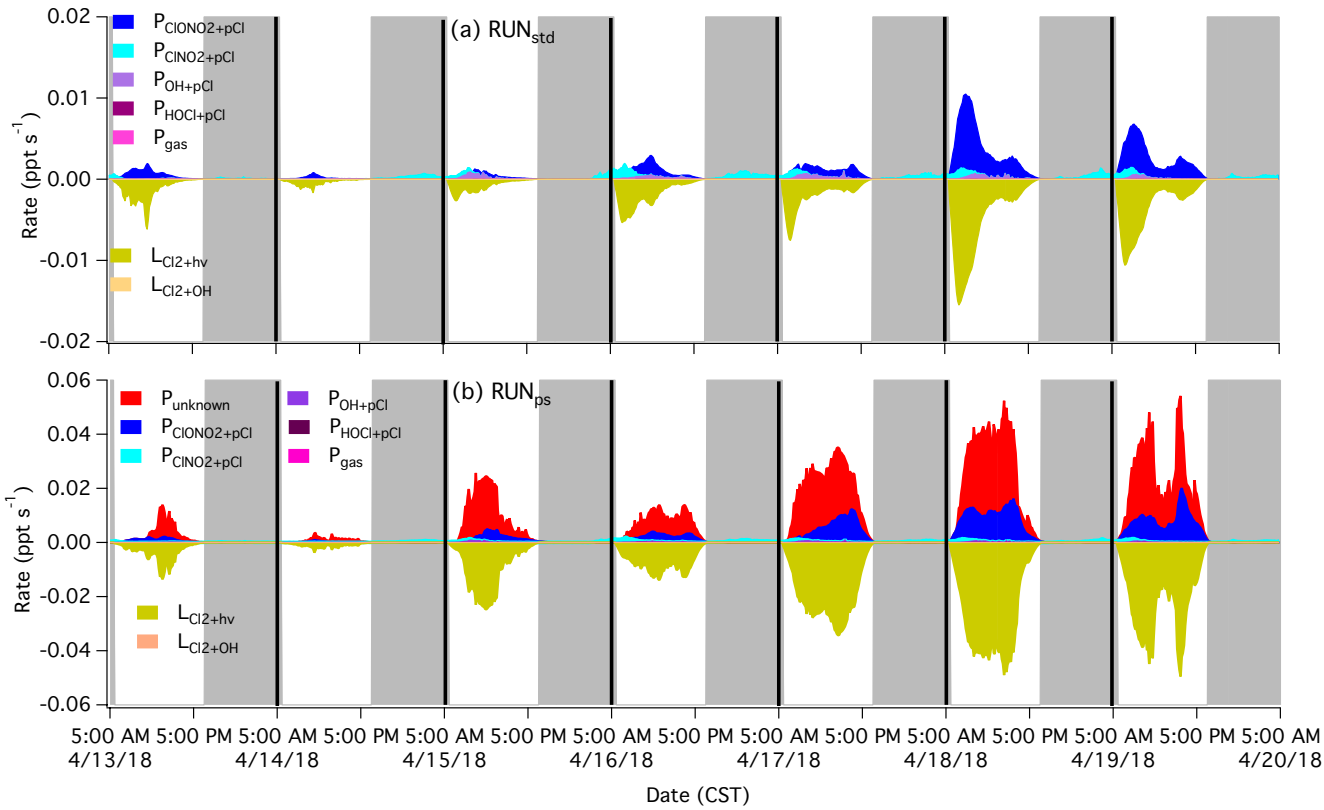

Figure 3. The production and loss rates of Cl_2 in (a) RUN_{std} and (b) RUN_{ps}. Each case day simulation starts at 05:00 a.m. $P_{ClONO2+pCl}$, $P_{ClNO2+pCl}$, P_{OH+pCl}, $P_{HOCl+pCl}$, and P_{gas} refer to Cl_2 production rates from uptake of $ClONO_2$, $ClNO_2$, OH, HOCl by aerosols, and gas-phase reactions, respectively. $P_{unknown}$ refers to the prescribed (missing) daytime Cl_2 source. L_{Cl2+hv} and L_{Cl2+OH} refer to Cl_2 loss rate due to photolysis and OH oxidation, respectively. The gray shading represents nighttime periods.

which chlorine species and HO_x come into steady state (Figures S1–S4 in Supporting Information S1). The model results on the third model day were used for analysis. The modeled Cl_2 concentrations at 05:00 a.m. on the third model day were constrained by observations (Figure 2; Suporting Information).

In addition, we found the model underestimates daytime Cl_2 observations in RUN_{std}, and then estimated the daytime Cl_2 missing source ($P_{unknown}$) that is needed to explain observations. The nighttime Cl_2 source has been discussed in Xia et al. (2020) and is small (on the order of 0.0001–0.001 ppt s^{-1}) compared to that during daytime (on the order of 0.01 ppt s^{-1}; Figure 3b), and thus is not repeated here. For the calculation of $P_{unknown}$, we first ran the standard model with the observed Cl_2 and $ClNO_2$ as well as HCl predicted from the E-AIM model as constraints, and obtained the "best estimates" of Cl, ClO, ClOO, OClO, Cl_2O_2, HOCl, and $ClONO_2$. Then we ran the model again but with these best estimated chlorine species as constraints, along with the observed $ClNO_2$ and E-AIM predicted HCl, to obtain the theoretical Cl_2. Then $P_{unknown}$ was estimated as: $P_{unknown} = j_{Cl2}$ (observed Cl_2 − theoretical Cl_2), assuming photochemical steady state of Cl_2 during daytime and its main loss through photolysis. j_{Cl2} is the photolysis frequency of Cl_2 corrected based on observed j_{NO2} with the factor j_{corr}. In order to evaluate the impacts of the daytime Cl_2 missing source ($P_{unknown}$) on the chlorine cycle and to compare it with the traditional daytime Cl_2 formation mechanisms in the same model scenario, we added $P_{unknown}$ to the standard model in the prescribed-source simulations (RUN_{ps}). As shown in Figure 2f, the model is able to reproduce daytime Cl_2 observations in RUN_{ps}, supporting the reasonable assumption made in calculating $P_{unknown}$.

A series of sensitivity model simulations were performed (Table S4 in Supporting Information S1). We increased HOCl mixing ratios by two orders of magnitude in the standard model ($RUN_{100HOCl}$) to test the sensitivity of Cl_2 production from aerosol uptake of HOCl. We used $\gamma_{ClNO2} = 6 \times 10^{-3}$ in the standard model ($RUN_{gammaClNO2}$) to test the sensitivity of Cl_2 production from aerosol uptake of $ClNO_2$. In another sensitivity model simulation, we added aerosol uptake of O_3 in the standard model (RUN_{O3}) to test the potential impacts of O_3, with three different uptake coefficient γ_{O3}: 1×10^{-5} (deliquesced NH_4Cl aerosols in the presence of SOA), 1×10^{-4} (intermediate case run),

and 1×10^{-3} (deliquesced NH_4Cl aerosols), based on Faxon et al. (2018; Section 3.3.4). In addition, we conduct a set of sensitivity simulations (RUN_{std_NOx} and RUN_{ps_NOx}) by using the family conservation of NO_x within F0AM that holds NO_x constant (based on observed $NO_x = NO_2 + NO$) while allowing NO_2 and NO to evolve freely within the 10-min time step. We conduct another set of sensitivity simulations (RUN_{std_VOCs} and RUN_{ps_VOCs}) by scaling the GC-MS VOCs (C_2H_4, C_2H_6, C_3H_6, C_3H_8, NC_4H_{10}, IC_4H_{10}, NC_5H_{12}, IC_5H_{12}, NC_6H_{14}, EBENZ, MXYL, OXYL, and PXYL) with the 10-min CO mixing ratio pattern. We conduct another set of sensitivity simulations (RUN_{std_nodil} and RUN_{ps_nodil}) by not considering the dilution/advection/deposition effects. The comparison of different model setup is shown in Table S4 in Supporting Information S1.

3. Results and Discussion

3.1. Cl_2 Observations

During the 1-week study period, Cl_2 generally dropped upon sunrise due to photolysis and accumulated at night (Figure 2f). The average observed Cl_2 mixing ratio was 13 ± 9 ppt (1σ) around noon (10:00–15:00) and 33 ± 20 ppt from midnight to sunrise (00:00–05:00), respectively. The first 2 days experienced weaker ($p < 0.05$) sunlight intensity (average j_{NO2}: 0.0026 ± 0.0015 s^{-1} around noon) compared to the last 3 days (average j_{NO2}: 0.0068 ± 0.0005 s^{-1} around noon). Despite stronger photolysis, Cl_2 was three times higher ($p < 0.05$) during the last 3 days (on average 20 ± 8 ppt around noon), compared to the first 2 days (on average 5 ± 2 ppt around noon), indicating higher Cl_2 production rate at stronger sunlight intensity. High levels of Cl_2, peaking at ~100 ppt around noon and dropping to ~40 ppt at midnight, have previously been observed at a rural site in the North China Plain, indicating strong daytime production of Cl_2 (Liu et al., 2017). In addition, high levels of daytime Cl_2 were also observed in coastal polluted regions (up to 1 ppb; Finley & Saltzman, 2008; Peng, Wang, Wang et al., 2021) and over coastal Arctic snowpack (up to 400 ppt; Liao et al., 2014). The exact chemical mechanisms contributing to large Cl_2 production during daytime are still unclear.

3.2. Modeling Cl_2 With Traditional Mechanisms

3.2.1. Modeled Versus Observed Cl_2

Cl_2 is significantly underestimated in the standard model run (RUN_{std}; Figure 2f), which is driven by traditional Cl_2 production mechanisms including uptake of $ClONO_2$, $ClNO_2$, HOCl, and OH by aerosols (Equations R4–R7) and gas-phase reactions $ClONO_2 + Cl$, $ClO + ClO$, and $ClOO + Cl$ (Equations R1–R3). In particular, the modeled Cl_2 is on average only 11% and 24% of observed Cl_2 around noon (10:00–15:00) and from midnight to sunrise (00:00–05:00), respectively, during the 1-week study period. The low Cl_2 around noon (1 ± 2 ppt) in RUN_{std} is consistent with previous GEOS-Chem modeling study showing model's inability to simulate daytime Cl_2 mixing ratio >1 ppt during the WINTER aircraft campaign over the eastern United States (Wang et al., 2019), suggesting an underestimate of daytime Cl_2 production in the model.

In RUN_{std}, over the 1-week study period, most (86%) of the Cl_2 is produced during daytime (05:40–18:40; Figure 3a). During daytime, uptake of $ClONO_2$ by aerosols ($P_{ClONO2+pCl}$) represents the biggest (80%) Cl_2 source, followed by uptake of $ClNO_2$ ($P_{ClNO2+pCl} = 10\%$) and OH ($P_{OH+pCl} = 10\%$) by aerosols; uptake of HOCl by aerosols ($P_{HOCl+pCl}$) and gas-phase mechanisms (P_{gas}) contribute <1% of Cl_2 formation. During nighttime (18:40–05:40), on the other hand, uptake of $ClNO_2$ by aerosols becomes the dominant (97%) Cl_2 source, followed by uptake of OH (2%) and $ClONO_2$ by aerosols (1%).

3.2.2. Sensitivities of Traditional Cl_2 Formation Mechanisms

In this section we will discuss the uncertainties of traditional Cl_2 formation mechanisms, including uptake of $ClONO_2$, $ClNO_2$, HOCl, and OH by aerosols, and examine whether these uncertainties can reconcile the discrepancy between the observed and modeled Cl_2 in the standard model run (RUN_{std}).

3.2.2.1. Uptake of $ClONO_2$ by Aerosols

The modeled $ClONO_2$, produced solely from reaction of ClO with NO_2, is <7 ppt in RUN_{std} (Figure 2d). $ClONO_2$ could have been underestimated in RUN_{std}, due to the underestimate of Cl_2 and subsequent underestimates of Cl and ClO, resulting in an underestimate of Cl_2 production rate from aerosol uptake of $ClONO_2$. The modeled $ClONO_2$ increases up to 22 ppt in the model run where daytime Cl_2 is well simulated (RUN_{ps}; Figure 2d). Note

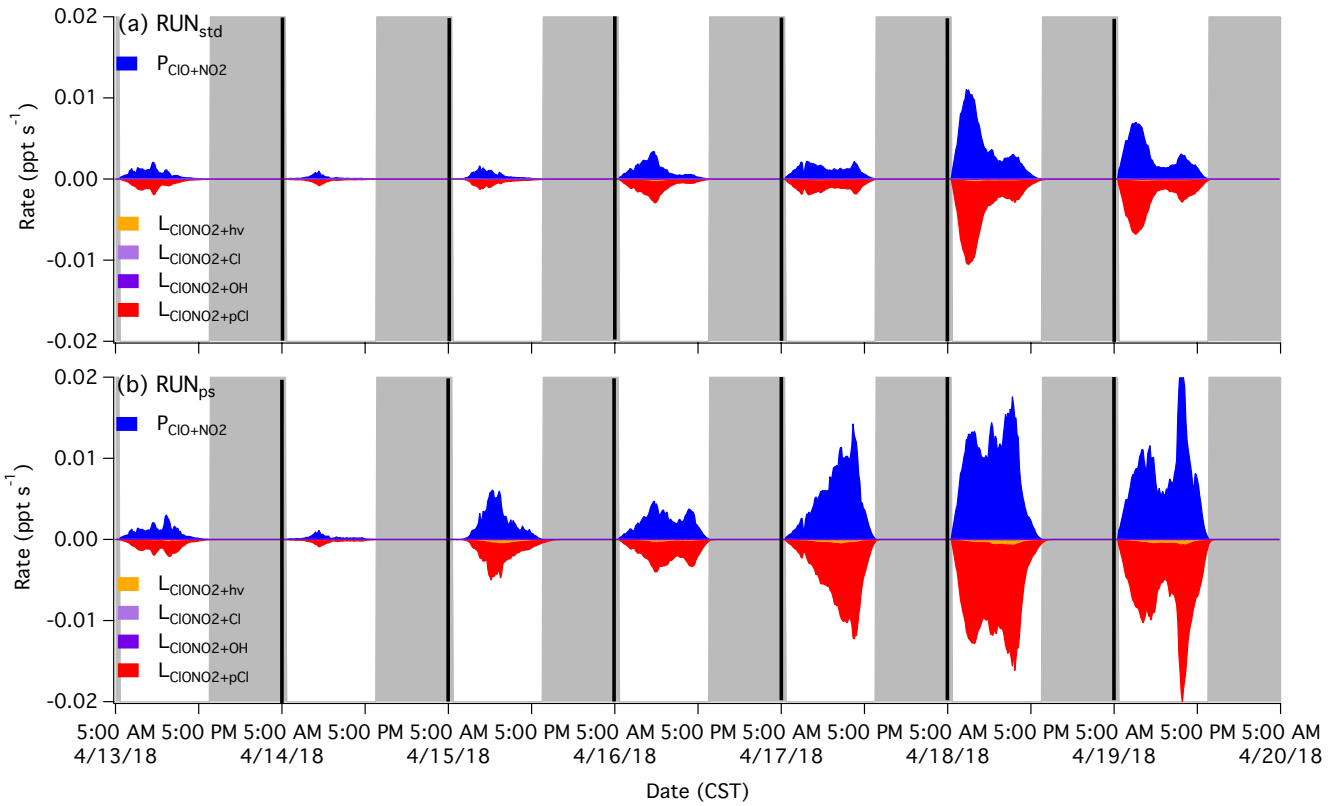

Figure 4. The production and loss rates of $ClONO_2$ in (a) RUN_{std} and (b) RUN_{ps}. Each case day simulation starts at 05:00 a.m. $P_{ClO+NO2}$ refers to $ClONO_2$ production rate from $ClO+NO_2$ reaction. $L_{ClONO2+hv}$, $L_{ClONO2+Cl}$, $L_{ClONO2+OH}$, and $L_{ClONO2+Cl}$ refer to $ClONO_2$ loss rate due to photolysis, Cl oxidation, OH oxidation, and aerosol uptake, respectively. The gray shading represents nighttime periods.

that the modeled $ClONO_2$ peaked during daytime in both RUN_{std} and RUN_{ps}. In comparison, in a previous field campaign at a semi-rural site in Beijing, the observed raw $ClONO_2$ signals peaked at night and reached minimum around noon (Le Breton et al., 2018). They hypothesized that ClO was rapidly converted to HOCl rather than $ClONO_2$ in extremely high OH and HO_2 mixing ratios. Unfortunately, $ClONO_2$ was not monitored in this study. Field measurements of $ClONO_2$ in the future will be useful to better constrain the Cl_2 formation mechanisms.

Even in the model run where daytime Cl_2 is well simulated (RUN_{ps}), the uptake of $ClONO_2$ by aerosols can only explain 29% of daytime Cl_2 production, as shown later in Section 3.3 and Figure 3b. The γ_{ClONO2} used in the model is 2.4×10^{-2}, following previous experimental results [$(2.44 \pm 0.23) \times 10^{-2}$ on 0.1 M aqueous NaCl droplets and $(2.41 \pm 0.20) \times 10^{-2}$ on pure water droplets] from Deiber et al. (2004). With $\gamma_{ClONO2} = 2.4 \times 10^{-2}$ in the model, the dominant sink of $ClONO_2$ is uptake by aerosols (Figure 4), meaning even an increase of γ_{ClONO2} (by unknown reasons) will not lead to an increase of Cl_2 production (or $ClONO_2$ removal) as the $ClO + NO_2$ reaction will set the $ClONO_2$ production limit. In a sensitivity simulation (RUN_{std_NOx}) using the family conservation of NO_x within F0AM, the modeled Cl_2 around noon is on average about 30% lower than that in RUN_{std} (Table S4), because the model (RUN_{std_NOx}) underestimates daytime NO_2 observations (or overestimates NO observations) on average by 1.6 ppb (FigureS5) and thus results in lower $ClONO_2$.

3.2.2.2. Uptake of $ClNO_2$ by Aerosols

The observed $ClNO_2$ was used as constraints in the model (Figure 2e). The calculated γ_{ClNO2} in this study (Section 2.2) is on average $(9 \pm 5) \times 10^{-6}$, within the range of 6×10^{-6}–7×10^{-5} derived from the WINTER aircraft campaign (Haskin et al., 2019). This is three orders of magnitude lower than that (6×10^{-3} over a deliquesced mixture of NaCl and oxalic acid with pH ≈ 1.8 and $[Cl^-] \approx 0.05$ M) obtained from Roberts et al. (2008), because the acid-catalyzed $ClNO_2 + Cl^-$ reaction is volume-limited with a reacto-diffusive length scale of 15 μm (Haskin et al., 2019). We perform a sensitivity run by using $\gamma_{ClNO2} = 6 \times 10^{-3}$ ($RUN_{gammaClNO2}$). In $RUN_{gammaClNO2}$, the model still frequently underestimates observed Cl_2 during daytime and it significantly overestimates observed

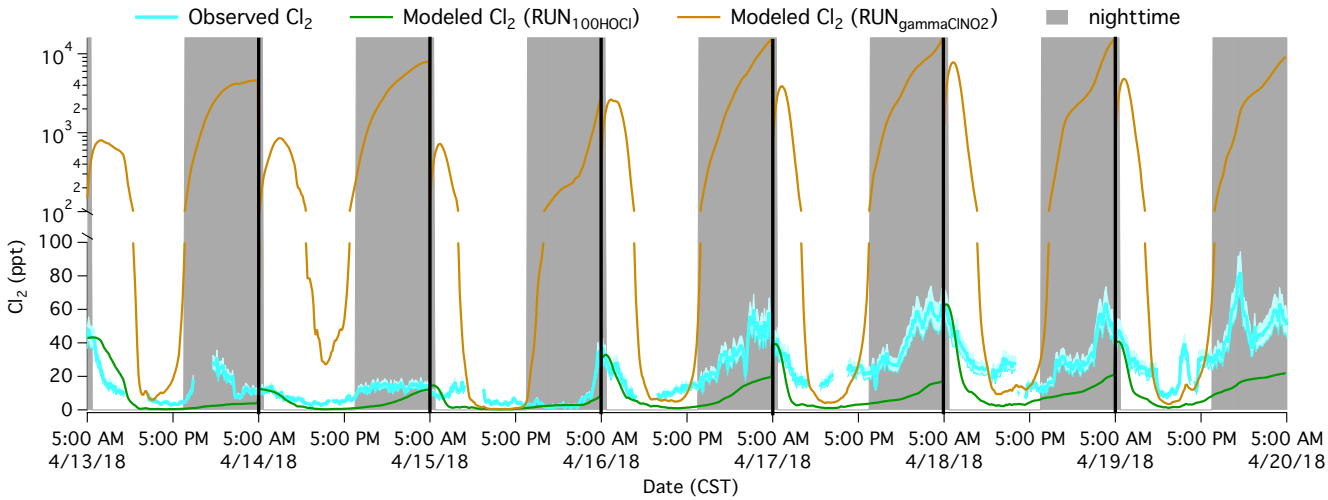

Figure 5. Observed Cl_2 (±15% uncertainties) and modeled Cl_2 mixing ratios in the sensitivity run with 100 times of HOCl in RUN_{std} ($RUN_{100HOCl}$) and fixed $\gamma_{ClNO2} = 6 \times 10^{-3}$ ($RUN_{gammaClNO2}$). Each case day simulation starts at 05:00 a.m. The gray shading represents nighttime periods.

Cl_2 at night with modeled Cl_2 reaching unrealistically high levels (>10 ppb; Figure 5). In this study, the observed $ClNO_2$ is much lower around noon (52 ± 46 ppt on average) than at night (1,000 ± 845 ppt on average), and the strong Cl_2 photolysis sink does not occur at night. Thus, it is unlikely for aerosol uptake of $ClNO_2$ to be an important daytime Cl_2 source, because otherwise it will produce even more Cl_2 at night, contradicting the fact that most Cl_2 is produced during daytime rather than nighttime (Figure 3).

3.2.2.3. Uptake of HOCl by Aerosols

The modeled HOCl is low (<1 ppt) in RUN_{std} (Figure 2c), mainly due to high levels of NO_2 and NO that remove ClO available for HOCl formation at our site. However, there could exist unknown photolytic HOCl sources, for example, initiated from oxidation of aerosol Cl^- via organic photosensitization (Jammoul et al., 2009; Lawler et al., 2011), that are missing in the model, as indicated from previous modeling studies that underestimated HOCl observations in the marine boundary layer (Lawler et al., 2011) and during the WINTER aircraft campaign over eastern US (Wang et al., 2019). Unfortunately, HOCl was not quantified in our study because its isotopic signals were not monitored by the CIMS and it was not calibrated (Xia et al., 2020). In comparison, Priestley et al. (2018) measured daytime HOCl mixing ratios to be <4 ppt in an urban environment in northern Europe where daytime Cl_2 mixing ratio was <10 ppt. The calculated γ_{HOCl} is on average (7 ± 12) × 10^{-4} in this study, in agreement with previous studies (4–18 × 10^{-4}; Lawler et al., 2011; Pratte & Rossi, 2006). As a sensitivity run, we increased HOCl mixing ratio by two orders of magnitude (upper limit; Simpson et al., 2015) in the standard model ($RUN_{100HOCl}$). The model still significantly underestimated observed Cl_2 in $RUN_{100HOCl}$ (Figure 5), with only 2 ± 2 ppt on average around noon, compared to 13 ± 9 ppt observed, suggesting aerosol uptake of HOCl is probably not the main daytime Cl_2 formation mechanism at our site.

3.2.2.4. Uptake of OH by Aerosols

The modeled daily maximum OH reaches (2–7) × 10^6 molecules cm^{-3} around noon in RUN_{std}, in agreement with previous observations made in the urban environment in China and around the world ((2–15) × 10^6 molecules cm^{-3}; Lu et al., 2019). The γ_{OH} (=0.04[Cl^-]) was calculated following Knipping and Dabdub (2002), with an average [Cl^-] of 0.4 ± 0.3 M. The Cl_2 production rate from aerosol uptake of OH (1 × 10^{-4} ppt s^{-1} on average) in RUN_{std} is two orders of magnitude lower than the observed Cl_2 removal rate (1 × 10^{-2} ppt s^{-1} on average) during daytime. That means, in order to reconcile the discrepancy between observed and modeled Cl_2 in RUN_{std}, the modeled OH concentrations need to be two orders of magnitude higher, which is not realistic.

3.3. Daytime Cl_2 Missing Source and Potential Causes

3.3.1. Daytime Cl_2 Missing Source

We estimated the daytime Cl_2 missing source ($P_{unknown}$) that is needed to reconcile the difference between modeled Cl_2 in RUN_{std} and observations (Section 2.2). Then we implemented this missing source into the model (RUN_{ps}), so that we can compare it with traditional mechanisms in the same model scenario. The modeled Cl_2 matches observed Cl_2 better in RUN_{ps} than RUN_{std} (Figure 2), especially around noon (on average 13 ± 8 ppt; not significantly different ($p > 0.05$) from observations), supporting the reasonable estimate of $P_{unknown}$. The normalized mean bias of Cl_2 ($N_{MB} = \frac{\sum_{i=1}^{n}(M_i - O_i)}{\sum_{i=1}^{n} O_i} \times 100\%$, where M_i and O_i are modeled value and observed value, respectively), is 3% during daytime and −38% during nighttime in RUN_{ps}, compared to −57% during daytime and −75% during nighttime in RUN_{std}. The improved model performance of daytime Cl_2 in RUN_{ps}, compared to RUN_{std}, has led to improved model performance of nighttime Cl_2. The nighttime Cl_2 source, as discussed in Xia et al. (2020) and thus not repeated here, is small (on the order of 0.0001–0.001 ppt s^{-1}) compared to the daytime Cl_2 source (on the order of 0.01 ppt s^{-1}; Figure 3b). In RUN_{ps}, over the 1-week study period, 98% of Cl_2 is produced during daytime, with $P_{unknown}$ constituting 68% of daytime Cl_2 production (Figure 3b). For each case day, $P_{unknown}$ accounts for 69%, 70%, 79%, 66%, 72%, 65%, and 65% of daytime Cl_2 production on April 13, 14, 15, 16, 17, 18, and 19, respectively; the average $P_{unknown}$ for the seven case days is (69 ± 5)%. The uptake of $ClONO_2$ by aerosols ($P_{ClONO2+pCl}$) accounts for 29% of daytime Cl_2 production, while uptake of $ClNO_2$ ($P_{ClNO2+pCl}$), OH (P_{OH+pCl}), and HOCl ($P_{HOCl+pCl}$) by aerosols and gas-phase mechanisms (P_{gas}) constitute <3% of daytime Cl_2 production, in RUN_{ps} during the 1-week study period.

The daytime Cl_2 missing source may be related to many environmental factors and it is difficult to isolate each of them in this study. By comparing the correlations between $P_{unknown}$ and individual environmental factors, including j_{NO2} ($R^2 = 0.66$), aerosol surface area concentration (SA; $R^2 = 0.28$), $PM_{2.5}$ mass concentration ($R^2 = 0.13$), chloride molar concentration [Cl^-] in $PM_{2.5}$ ($R^2 = 0.001$), aerosol acidity ([H^+] concentration in $PM_{2.5}$; $R^2 = 0.002$), SO_2 ($R^2 = 0.23$), CO ($R^2 = 0.02$), and O_3 mixing ratios ($R^2 = 0.13$), we found that $P_{unknown}$ shows the strongest correlation with j_{NO2} (Figure S7 in Supporting Information S1). Furthermore, the correlations between $P_{unknown}$ and different environmental factors multiplied by j_{NO2} are shown in Figure 6. Compared to the correlation of $P_{unknown}$ versus j_{NO2} ($R^2 = 0.66$), the correlations of $P_{unknown}$ versus $j_{NO2} \times SA$ ($R^2 = 0.84$), $P_{unknown}$ versus $j_{NO2} \times PM_{2.5}$ ($R^2 = 0.78$), $P_{unknown}$ versus $j_{NO2} \times SO_2$ ($R^2 = 0.70$), and $P_{unknown}$ versus $j_{NO2} \times CO$ ($R^2 = 0.74$) all improve, suggesting other factors in addition to sunlight intensity also affect $P_{unknown}$. Below we discuss the potential mechanisms that may explain $P_{unknown}$, including the Fe^{3+}-induced photolytic Cl_2 formation mechanism, bulk aerosol $OH_{(aq)}$ oxidation mechanism, and uptake of O_3 by aerosols.

3.3.2. Iron(III)-Induced Photolytic Cl_2 Formation Mechanism

The Fe^{3+}-induced photolytic Cl_2 formation mechanism (Equations R9–R14) proposed by previous laboratory studies (Lim et al., 2006; Wittmer, Bleicher, Ofner, & Zetzsch, 2015; Wittmer, Bleicher, & Zetzsch, 2015) may serve as a daytime Cl_2 source not considered in the standard model. When Fe^{3+} and Cl^- are both present in aerosols, photolysis of $FeCl^{2+}$ and $FeCl_2^+$ generates aqueous-phase $Cl_{(aq)}$ radicals (Equations R9–R10), which react rapidly with Cl^- to form Cl_2^- radicals (Equation R11). Cl_2^- reacts with $Cl_{(aq)}$ (Equation R12) or another Cl_2^- (Equations R13 and R14) to produce Cl_2. The initial step, photolysis of $FeCl^{2+}$ and $FeCl_2^+$, is light dependent, consistent with the positive correlation between $P_{unknown}$ and j_{NO2} ($R^2 = 0.66$; Figure 6a). Better correlation is found between $P_{unknown}$ and $j_{NO2} \times PM_{2.5}$ ($R^2 = 0.78$, Figures 6c) and $j_{NO2} \times SA$ ($R^2 = 0.84$, Figure 6b), supporting Fe^{3+}-induced Cl_2 formation within the aerosols. Weaker correlation is found between $P_{unknown}$ and $j_{NO2} \times [Cl^-]$ ($R^2 = 0.27$, Figure 6d), suggesting the daytime Cl_2 missing source does not necessarily increase with chloride concentration (Figure S7d in Supporting Information S1). Interestingly, for the four clear-sky case days (April 15 and April 17–19) with very similar average daytime j_{NO2} (0.0045–0.0049 s^{-1}), average daytime $P_{unknown}$ remains relatively unchanged at particle chloride concentration ([Cl^-]) of 0.2–0.4 M but decreases when [Cl^-] rises to 0.6 M (Figure S8d in Supporting Information S1), consistent with experimental results from Lim et al. (2006). This is due to a shift from $FeCl^{2+}$ (higher $Cl_{(aq)}$ quantum yield) to $FeCl_2^+$ (lower $Cl_{(aq)}$ quantum yield) at high [Cl^-] (Lim et al., 2006; Nadtochenko & Kiwi, 1998).

Neither aerosol Fe nor Fe^{3+} concentrations were measured in this study. But high aerosol Fe concentrations (~1 μg m^{-3}) have been observed in Nanjing (Wang et al., 2017) and other urban areas in East China (Zhu et al., 2020), mainly due to fossil fuel combustion and biomass burning emissions (Furutani et al., 2011; Zhu

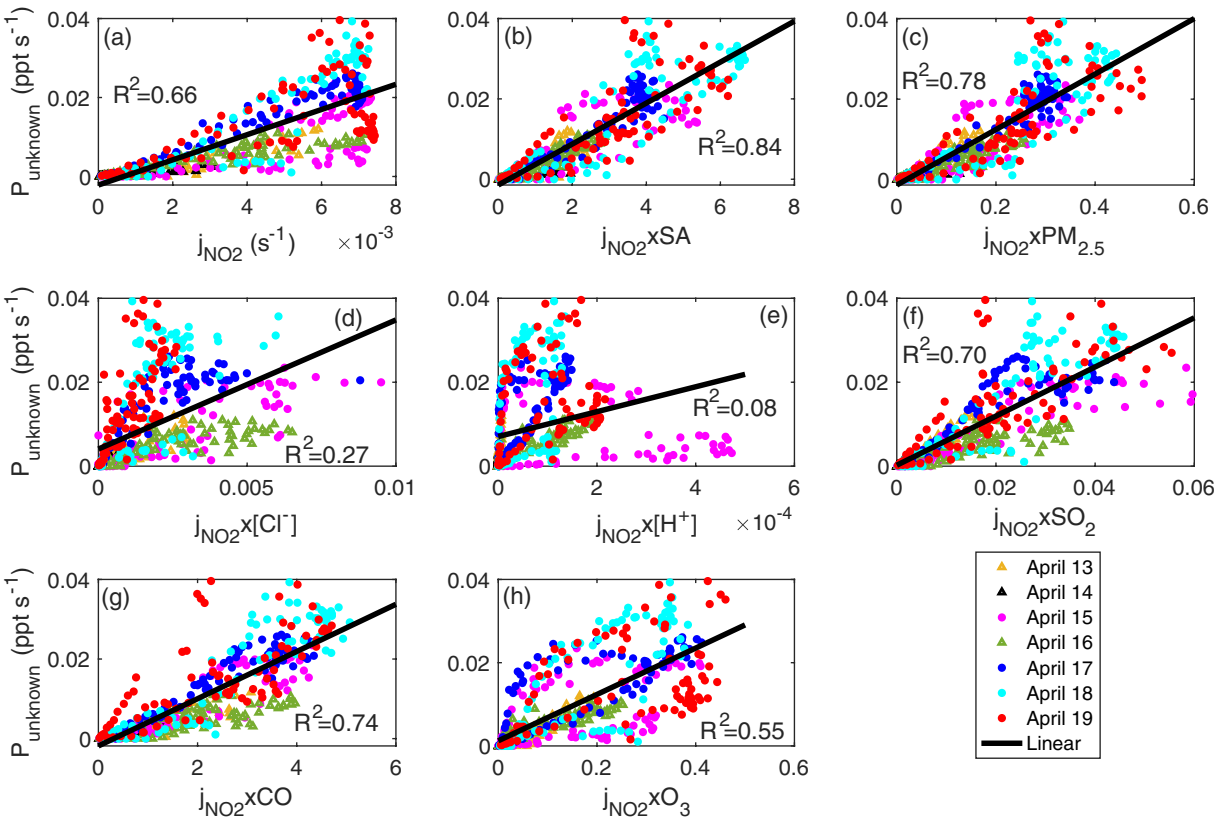

Figure 6. Correlations between daytime $P_{unknown}$ (10-min averages) and (a) j_{NO2} and (b)–(h) other different environmental factors multiplied by j_{NO2} for the seven case days. The environment factors include (a) j_{NO2} (s^{-1}), (b) aerosol surface area concentration (SA, $\mu m^2\ cm^{-3}$), (c) $PM_{2.5}$ mass concentration ($\mu g\ m^{-3}$), (d) chloride molar concentration (Cl^-) in $PM_{2.5}$ (mol l^{-1}), (e) aerosol acidity (H^+ concentration in $PM_{2.5}$; mol l^{-1}), (f) SO_2 (ppb), (g) CO (ppb), and (h) O_3 (ppb) mixing ratios. The least squares regression line ($y = ax + b$) for all the 10-min data is shown for each plot, with corresponding regression coefficient R^2.

et al., 2020). Previous modeling studies also suggested East China as a hotspot of anthropogenic Fe emissions (Alexander et al., 2009; Luo et al., 2008). Better correlation with $P_{unknown}$ is found when j_{NO2} is multiplied by SO_2 ($R^2 = 0.70$, Figure 6f) or CO ($R^2 = 0.74$, Figure 6g), indicators of coal combustion and biomass burning activities (potential Fe sources), again supporting Fe^{3+}-induced Cl_2 formation within the aerosols. Both the soluble Fe concentration and soluble Fe fraction showed a positive correlation with $PM_{2.5}$ concentration in East China in a previous study (Zhu et al., 2020). The soluble fraction of Fe in aerosols ($PM_{2.5}$) was observed to be 3%–5% in four urban sites in East China in December 2017 (Zhu et al., 2020). The fraction of Fe^{3+} in soluble Fe (Fe^{3+}/(Fe^{3+} + Fe^{2+})) for aerosols collected in the continental outflow of East China was observed to be about 67% (Moffet et al., 2012). The average daytime $PM_{2.5}$ Cl^- concentration is 0.4 ± 0.4 $\mu g\ m^{-3}$ during the study period. As a result, the aerosol Cl^-/Fe^{3+} ratio is estimated to range from 17–28 mol mol^{-1} during the study period (at average aerosol pH of 2.3 ± 0.8), consistent with previous experimental conditions under which Fe^{3+}-induced photolytic Cl_2 production occurred (Cl^-/Fe^{3+}: 13–101 mol mol^{-1}, aerosol pH: 1.9–4.2; Wittmer, Bleicher, Ofner, & Zetzsch, 2015). A quantitative expression of Cl_2 production rate using sunlight intensity, aerosol abundance, and Fe^{3+} and Cl^- concentrations is not available in previous laboratory studies, such that we are not able to quantify the Fe^{3+}-induced photolytic Cl_2 production in this study, and future investigation is needed. Nevertheless, the dependence of $P_{unknown}$ on j_{NO2}, $PM_{2.5}$, and aerosol surface area concentrations suggests aerosol photochemistry (possibly involving iron) could play an important role in daytime Cl_2 production at our suburban site in East China.

3.3.3. Bulk Aerosol $OH_{(aq)}$ Oxidation Mechanism

Another aerosol photochemistry related daytime Cl_2 formation pathway is through reaction of $OH_{(aq)}$ with Cl^- in the bulk aerosols (Equation R16) and subsequent formation of $Cl_{(aq)}$ radicals (Equations R17 and R18) and Cl_2 (Equations R11–R14), as proposed by Oum et al. (1998). However, model simulations suggested this bulk aerosol

$OH_{(aq)}$ oxidation mechanism underestimates Cl_2 production by more than three orders of magnitude in laboratory experiments when O_3 photolysis is the only aerosol $OH_{(aq)}$ source (Knipping & Dabdub, 2002; Knipping et al., 2000). Therefore, a gas-aerosol interface OH oxidation mechanism involving the formation of a relatively stable complex $(OH \cdots Cl^-)_{surface}$ (Equation R7) was proposed to explain experimental Cl_2 production (Knipping & Dabdub, 2002; Knipping et al., 2000). In fact, this gas-aerosol interface OH oxidation mechanism (Reaction TD4 in Table 1) has been implemented in our box model (RUN_{std}) but it is not able to explain the high daytime Cl_2 observed in the field (Figure 2), consistent with recent modeling studies (Qiu et al., 2019; Wang et al., 2019).

$$OH_{(aq)} + Cl^- \rightleftharpoons ClOH^- \quad \text{(R16)}$$

$$ClOH^- + H^+ \rightleftharpoons ClOH_{2(aq)} \quad \text{(R17)}$$

$$ClOH_{2(aq)} \rightarrow Cl_{(aq)} + H_2O \quad \text{(R18)}$$

There could exist other $OH_{(aq)}$ sources within aerosols that initiate Cl_2 production, including the photo-Fenton reactions ($Fe^{2+}/Cu^+ + H_2O_2$), as well as the photolysis of aerosol nitrate, nitrite, Fe^{3+}-hydroxy complexes ($FeOH^{2+}$, $Fe(OH)_2^+$), hydrogen peroxide (H_2O_2), organic peroxides (ROOH), and "colored" dissolved organic matter, as reviewed by Tilgner and Herrmann (2018). Whether these sources can supply a large amount of $OH_{(aq)}$ for Cl_2 formation is currently unknown and necessitates future investigation. It should be noted that $P_{unknown}$ does not show good correlation with $j_{NO2} \times [H^+]$ ($R^2 = 0.08$, Figure 6e) or $[H^+]$ ($R^2 = 0.002$, Figure S7e in Supporting Information S1), indicating the daytime Cl_2 missing source in this study does not depend on aerosol acidity, which is needed in the $OH_{(aq)}$ oxidation mechanism (Equations R16–R18).

3.3.4. Uptake of O_3 by Aerosols

Uptake of O_3 by aerosols has been proposed as a potential Cl_2 formation pathway (Faxon et al., 2018; Qiu et al., 2019; Sadanaga et al., 2001), though good correlation between $P_{unknown}$ and O_3 mixing ratio is not found in this study ($R^2 = 0.13$, Figure S7h in Supporting Information S1). Production of Cl_2 was observed in previous laboratory experiments when O_3 was exposed to chloride-containing aerosols both in the presence of light (Faxon et al., 2018; Knipping et al., 2000; Laskin et al., 2006; Oum et al., 1998), with OH scavenger (cyclohexane; Faxon et al., 2018), and under dark conditions (Abbatt & Waschewsky, 1998; Faxon et al., 2018; Sadanaga et al., 2001). The uptake of O_3 by deliquesced NaCl aerosols is very slow ($\gamma_{O3} < 1 \times 10^{-4}$; Abbatt & Waschewsky, 1998). However, Sadanaga et al. (2001) found γ_{O3} increased by several orders of magnitude when NaCl was mixed with $FeCl_3$, reaching 3.6×10^{-2} and 3.4×10^{-2} when Fe/Na weight ratio was 1.0% and 0.5%, with a Cl_2 yield of 0.48 and 0.28, respectively. Their results suggested aerosol uptake of O_3 and subsequent production of Cl_2 could be catalyzed by trace metals (Fe^{3+}). More recently, Faxon et al. (2018) measured γ_{O3} to be 1×10^{-3} on deliquesced NH_4Cl aerosols but only 1×10^{-5} in the presence of SOA in their chamber experiments.

As a sensitivity study, we added the O_3 uptake mechanism into the standard model (RUN_{O3}), with three different γ_{O3}: 1×10^{-5} (deliquesced NH_4Cl aerosols in the presence of SOA), 1×10^{-4} (intermediate case run), and 1×10^{-3} (deliquesced NH_4Cl aerosols), based on Faxon et al. (2018). Note that the particle sodium (Na^+) concentrations were below detection limit and the particle ammonium (NH_4^+) concentrations were on average 5 ± 3 μg m^{-3} during the study period. With $\gamma_{O3} = 1 \times 10^{-5}$, the model generally reproduces observed Cl_2 during daytime, especially around noon (11 ± 8 ppt modeled vs. 13 ± 9 observed), but overestimates observed nighttime Cl_2 by a factor of 6 on average (Figure 7) due to a lack of strong photolysis sink at night. With $\gamma_{O3} = 1 \times 10^{-4}$ or 1×10^{-3}, the model significantly overestimate observed Cl_2, reaching 100 ± 68 and 987 ± 660 ppt around noon, respectively (Figure 7). Recently, Qiu et al. (2019) used $\gamma_{O3} = 1 \times 10^{-3}$ during daytime and $\gamma_{O3} = 1 \times 10^{-5}$ during nighttime in the three-dimensional Community Multiscale Air Quality (CMAQ) model to investigate chlorine chemistry impacts on air quality in North China, but the rationale for choosing these vales was not given. The aerosol uptake of O_3 accounts for more than 80% of Cl_2 production in their model, which reproduces ~100 ppt of noontime Cl_2 observed at the Wangdu site in North China. However, the high γ_{O3} used in their model are not applicable at our site, due to large overestimate of observed Cl_2 (Figure 7). In addition, the correlation with $P_{unknown}$ gets weaker when SA is multiplied by O_3 (comparing Figure S7b with Figure S12a in Supporting Information S1) or when $j_{NO2} \times SA$ is multiplied by O_3 (comparing Figure 6b with Figure S12b in Supporting Information S1), suggesting the daytime Cl_2 missing source is more likely to be caused by aerosol photochemistry rather than aerosol uptake of O_3.

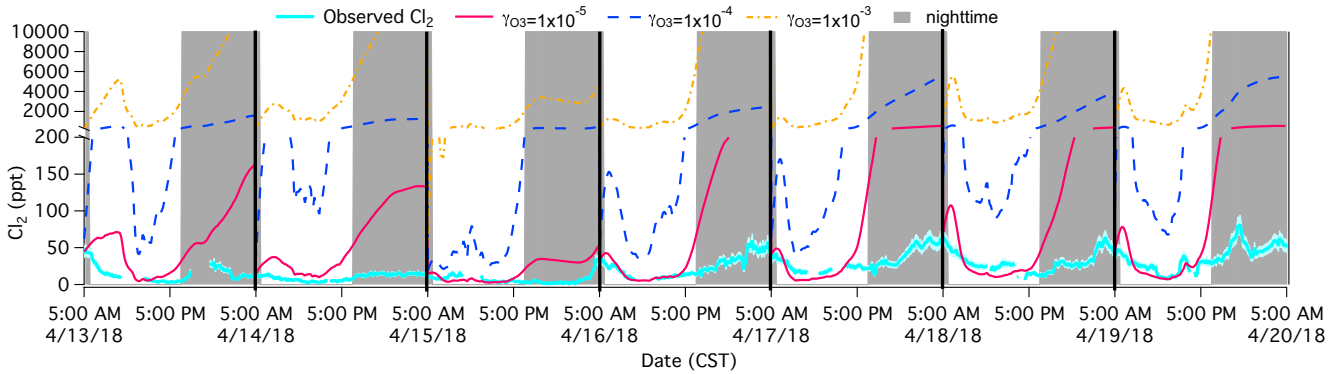

Figure 7. Observed Cl_2 (±15% uncertainties) and modeled Cl_2 mixing ratios in the sensitivity run considering uptake of O_3 by aerosols (RUN_{O3}) with three different γ_{O3}: 1×10^{-5}, 1×10^{-4}, and 1×10^{-3}. Each case day simulation starts at 05:00 a.m. The gray shading represents nighttime periods.

3.3.5. Anthropogenic Source of Cl_2

Anthropogenic activities, such as coal combustion, water treatment (usage of chlorine-containing disinfectants), waste water treatment, waste incineration, and industrial processes, have been proposed as potential sources of Cl_2 in the atmosphere, though their emission fluxes are not well known (Chang et al., 2002; Liu et al., 2018; Riedel et al., 2012, 2013; Tanaka et al., 2000; Yi et al., 2021). Riedel et al. (2012) observed up to 200 ppt Cl_2 at night when sampling the Los Angeles urban plume on a research vessel and proposed localized industrial emissions of reactive chlorine. Furthermore, Riedel et al. (2013) observed up to 320 ppt Cl_2 at night from urban or power plant plumes on a tall tower in a polluted continental site in Weld County, Colorado and proposed direct emissions from nearby power plants/cooling towers/waste disposal/incineration. Liu et al. (2017) and Peng, Wang, Xia et al. (2021) observed elevated levels of Cl_2 (up to 450 ppt during daytime) in Wangdu (North China), where coal combustion for power plants and residential heating and cooking was widespread. However, none of these studies quantified the contribution of direct anthropogenic emission to the Cl_2 budget and the difference between daytime and nighttime.

In this study, our sampling site was surrounded mainly by teaching and residential buildings, vegetation, and sparse roads within 1–2 km, and we do not expect significant local anthropogenic emission of Cl_2 (a lifetime of ~10 min at noon). The 9-m wind speed at the SORPES station was generally low (83% of the period below 3 m s^{-1}) during our 1-week study period and the wind direction was mainly (77% of the period) from the east (mainly vegetation cover) while downtown Nanjing was in the west (industrial and urban areas; Figure 1). In addition, the northwest wind that likely carried anthropogenic Cl_2 mainly occurred on April 14 and April 15 (Figure S6 in Supporting Information S1) when both nighttime and daytime Cl_2 mixing ratios were low (Figure 2), suggesting regional transport of direct anthropogenic emission of Cl_2 to our site is likely not significant during our study period. If large anthropogenic Cl_2 source arrived at our site during daytime especially around noon, one would expect an increase in particulate chloride concentration around noon as well, but this was not shown in the $PM_{2.5}$ chloride mass concentration data (FigureS6). Therefore, direct anthropogenic Cl_2 emission is likely not the main cause of the daytime Cl_2 missing source in this study.

3.4. Implication for Oxidation of VOCs

It is important to understand daytime Cl_2 formation, in order to better simulate the abundance of Cl radicals, a strong oxidant for volatile organic compounds (VOCs) in the atmosphere (Xue et al., 2015). In RUN_{ps}, over the 1-week study period, Cl_2 photolysis represents the biggest Cl radical source (50%), followed by $ClNO_2$ photolysis (46%) and reaction of ClO with NO (3%; Figure 8). Photolysis of $ClNO_2$ and Cl_2 is the biggest Cl radical source in the morning and in the afternoon, respectively (Figure 8). The daytime Cl mixing ratios are significantly higher in RUN_{ps} than RUN_{std} (Figure 2a), especially in the afternoon (on average a factor of 4 higher from noon to sunset). As a result, compared to RUN_{std}, the reactivities of ethane, propane, *n*-butane, *i*-butane, *n*-pentane, *i*-pentane, *n*-hexane, methanol, and ethanol in RUN_{ps} increase by 38%, 22%, 19%, 15%, 14%, 12%, 12%, 13%, and 7%, respectively. Air quality modeling studies considering only traditional Cl_2 formation mechanisms could underestimate Cl radical abundances and the oxidation of VOCs and production of O_3 and SOA (Qiu et al., 2019).

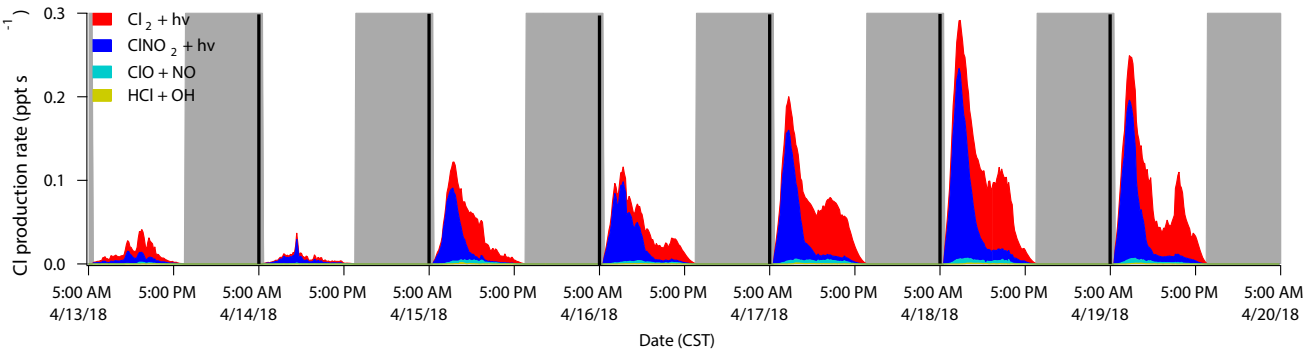

Figure 8. The production rates of Cl radicals form different pathways in RUN_{ps}. Each case day simulation starts at 05:00 a.m. The gray shading represents nighttime periods.

In addition, over the 1-week study period, the fraction of greenhouse gas CH_4 oxidized by Cl increases from 5% in RUN_{std} to 8% in RUN_{ps}. Due to the large kinetic isotope effect for reaction of CH_4 with Cl (Saueressig et al., 1995), a small change in the fraction of CH_4 oxidized by Cl can result in a large change in the carbon isotopes ($\delta^{13}C$) of CH_4. Thus, it is critical to have a good constraint on tropospheric Cl abundances, in order to use $\delta^{13}C$ of CH_4 to investigate CH_4 sources and sinks at the present day (Gromov et al., 2018; Strode et al., 2020) and in the past (e.g., Last Glacial Maximum; Bock et al., 2017; Ferretti et al., 2005; Hopcroft et al., 2018; Levine et al., 2011).

4. Conclusions

In this study, we investigate Cl_2 formation mechanisms at a suburban site in East China using a box model with detailed chlorine chemistry and comprehensive observational constraints. During the 1-week study period in April 2018, the observed Cl_2 was on average 13 ± 9 ppt around noon and reached higher levels during days with stronger sunlight intensity. The standard model run with traditional Cl_2 formation mechanisms, including uptake of $ClONO_2$, $ClNO_2$, HOCl, and OH by aerosols, can only reproduce on average 11% of the observed Cl_2 around noon, consistent with the large underestimate of daytime Cl_2 found in previous atmospheric chemical transport modeling studies (Qiu et al., 2019; Wang et al., 2019). The missing daytime Cl_2 source was estimated, accounting for on average (69 ± 5)% of daytime Cl_2 production for the seven case days. This missing daytime Cl_2 source correlates well with sunlight intensity and aerosol abundance, suggesting photochemistry within aerosols (e.g., Fe^{3+}-induced photochemistry or bulk $OH_{(aq)}$ oxidation) could play an important role in Cl_2 formation at our site, but future investigation is needed to elucidate relevant chemical mechanisms and quantify their contributions. The fast aerosol uptake of O_3, with an uptake coefficient of 1×10^{-3}, as proposed by a recent modeling study to investigate Cl_2 impacts on air quality in North China (Qiu et al., 2019), is not applicable at our site and the chlorine chemistry impacts on air quality should be revisited. With the missing daytime Cl_2 source added in the model, the chlorine radical abundance increases by a factor of four in the afternoon, enhancing VOCs (especially alkane) oxidation. This study highlights the large discrepancy between observed and modeled daytime Cl_2 with traditional Cl_2 formation mechanisms and the need for improved understanding of daytime Cl_2 formation through laboratory, modeling, and field studies. It is necessary to design laboratory experiments to quantify the Cl_2 production rate from for example, iron(III)-induced or $OH_{(aq)}$-initiated aerosol photochemistry. The laboratory-based Cl_2 production rate parameterization can be implemented into the box, regional, and global models to revisit reactive chlorine chemistry in the troposphere. More field measurements of Cl_2 along with other reactive chlorine species (e.g., HOCl and $ClONO_2$) in different environments are needed to evaluate the model performance.

Data Availability Statement

The data and chlorine chemistry mechanisms used in this study are available on the Zenodo platform (https://doi.org/10.5281/zenodo.5269033). The F0AM box model is available at https://github.com/AirChem/F0AM.

Acknowledgments
This study was supported by the Hong Kong Research Grants Council (Grant No. T24-504/17-N), Hong Kong PolyU Start-up Fund (Grant No. P0039258), National Natural Science Foundation of China (Grant Nos. 91544213, 41675145, 42075101, and 41922052), and Jiangsu Provincial Fund on $PM_{2.5}$ and O_3 Pollution Mitigation (Grant No. 2019023). Qianjie Chen acknowledges Glenn M. Wolfe for sharing the F0AM box model.

References

Abbatt, J. P. D., & Waschewsky, G. C. G. (1998). Heterogeneous interactions of HOBr, HNO_3, O_3, and NO_2 with deliquescent NaCl aerosols at room temperature. *The Journal of Physical Chemistry A*, *102*, 3719–3725. https://doi.org/10.1021/jp980932d

Alexander, B., Park, R. J., Jacob, D. J., & Gong, S. (2009). Transition metal-catalyzed oxidation of atmospheric sulfur: Global implications for the sulfur budget. *Journal of Geophysical Research: Atmospheres*, *114*, D02309. https://doi.org/10.1029/2008JD010486

Ammann, M., Cox, R. A., Crowley, J. N., Jenkin, M. E., Mellouki, A., Rossi, M. J., et al. (2013). Evaluated kinetic and photochemical data for atmospheric chemistry: Volume VI–heterogeneous reactions with liquid substrates. *Atmospheric Chemistry and Physics*, *13*(16), 8045–8228. https://doi.org/10.5194/acp-13-8045-2013

Baier, B. C., Brune, W. H., Miller, D. O., Blake, D., Long, R., Wisthaler, A., et al. (2017). Higher measured than modeled ozone production at increased NOx levels in the Colorado Front Range. *Atmospheric Chemistry and Physics*, *17*(18), 11273–11292. https://doi.org/10.5194/acp-17-11273-2017

Behnke, W., George, C., Scheer, V., & Zetzsch, C. (1997). Production and decay of ClNO2 from the reaction of gaseous N2O5 with NaCl solution: Bulk and aerosol experiments. *Journal of Geophysical Research: Atmospheres*, *102*(D3), 3795–3804. https://doi.org/10.1029/96JD03057

Bock, M., Schmitt, J., Beck, J., Seth, B., Chappellaz, J., & Fischer, H. (2017). Glacial/interglacial wetland, biomass burning, and geologic methane emissions constrained by dual stable isotopic CH4 ice core records. *Proceedings of the National Academy of Sciences of the United States of America*, *114*(29), E5778–E5786. https://doi.org/10.1073/pnas.1613883114

Chang, S., McDonald-Buller, E., Kimura, Y., Yarwood, G., Neece, J., Russell, M., et al. (2002). Sensitivity of urban ozone formation to chlorine emission estimates. *Atmospheric Environment*, *36*(32), 4991–5003. https://doi.org/10.1016/S1352-2310(02)00573-3

Chen, Q., Sherwen, T., Evans, M., & Alexander, B. (2018). DMS oxidation and sulfur aerosol formation in the marine troposphere: A focus on reactive halogen and multiphase chemistry. *Atmospheric Chemistry and Physics*, *18*, 13617–13637. https://doi.org/10.5194/acp-18-13617-2018

Deiber, G., George, C., Le Calvé, S., Schweitzer, F., & Mirabel, P. (2004). Uptake study of $ClONO_2$ and $BrONO_2$ by Halide containing droplets. *Atmospheric Chemistry and Physics*, *4*, 1291–1299. https://doi.org/10.5194/acp-4-1291-2004

Ding, A., Huang, X., Nie, W., Chi, X., Xu, Z., Zheng, L., et al. (2019). Significant reduction of $PM_{2.5}$ in eastern China due to regional-scale emission control: Evidence from SORPES in 2011–2018. *Atmospheric Chemistry and Physics*, *19*, 11791–11801. https://doi.org/10.5194/acp-19-11791-2019

Ding, A., Nie, W., Huang, X., Chi, X., Sun, J., Kerminen, V. M., et al. (2016). Long-term observation of air pollution-weather/climate interactions at the SORPES station: A review and outlook. *Frontiers of Environmental Science & Engineering*, *10*(5), 1–15. https://doi.org/10.1007/s11783-016-0877-3

Faxon, C. B., Dhulipala, S. V., Allen, D. T., & Hildebrandt Ruiz, L. (2018). Heterogeneous production of Cl_2 from particulate chloride: Effects of composition and relative humidity. *AIChE Journal*, *64*, 3151–3158. https://doi.org/10.1002/aic.16204

Ferretti, D. F., Miller, J. B., White, J. W. C., Etheridge, D. M., Lassey, K. R., Lowe, D. C., et al. (2005). Unexpected changes to the global methane budget over the past 2000 years. *Science*, *309*, 1714–1717. https://doi.org/10.1126/science.1115193

Finlayson-Pitts, B. J., Ezell, M. J., & Pitts, J. N. (1989). Formation of chemically active chlorine compounds by reactions of atmospheric NaCl particles with gaseous N2O5 and ClONO2. *Nature*, *337*(6204), 241–244. https://doi.org/10.1038/337241a0

Finley, B. D., & Saltzman, E. S. (2006). Measurement of Cl_2 in coastal urban air. *Geophysical Research Letters*, *33*, L11809. https://doi.org/10.1029/2006GL025799

Finley, B. D., & Saltzman, E. S. (2008). Observations of Cl_2, Br_2, and I_2 in coastal marine air. *Journal of Geophysical Research*, *113*, D21301. https://doi.org/10.1029/2008JD010269

Furutani, H., Jung, J., Miura, K., Takami, A., Kato, S., Kajii, Y., & Uematsu, M. (2011). Single-particle chemical characterization and source apportionment of iron-containing atmospheric aerosols in Asian outflow. *Journal of Geophysical Research*, *116*, D18204. https://doi.org/10.1029/2011JD015867

Gebel, M. E., & Finlayson-Pitts, B. J. (2001). Uptake and reaction of ClONO2 on NaCl and synthetic sea salt. *The Journal of Physical Chemistry A*, *105*(21), 5178–5187. https://doi.org/10.1021/jp0046290

Gromov, S., Brenninkmeijer, C. A. M., & Jöckel, P. (2018). A very limited role of tropospheric chlorine as a sink of the greenhouse gas methane. *Atmospheric Chemistry and Physics*, *18*, 9831–9843. https://doi.org/10.5194/acp-18-9831-2018

Haskin, J. D., Lee, B. H., Lopez-Hilifiker, F. D., Peng, Q., Jaeglé, L., Reeves, J. M., et al. (2019). Observational constraints on the formation of Cl2 from the reactive uptake of ClNO2 on aerosols in the polluted marine boundary layer. *Journal of Geophysical Research: Atmospheres*, *124*, 8851–8869. https://doi.org/10.1029/2019JD030627

Hopcroft, P. O., Valdes, P. J., & Kaplan, J. O. (2018). Bayesian analysis of the glacial-interglacial methane increase constrained by stable isotopes and Earth system modeling. *Geophysical Research Letters*, *45*, 3653–3663. https://doi.org/10.1002/2018GL077382

Hossaini, R., Chipperfield, M. P., Saiz-Lopez, A., Fernandez, R., Monks, S., Feng, W., et al. (2016). A global model of tropospheric chlorine chemistry: Organic versus inorganic sources and impact on methane oxidation. *Journal of Geophysical Research: Atmospheres*, *121*, 14271–14297. https://doi.org/10.1002/2016JD025756

Jammoul, A., Dumas, S., D'Anna, B., & George, C. (2009). Photoinduced oxidation of sea salt halides by aromatic ketones: A source of halogenated radicals. *Atmospheric Chemistry and Physics*, *9*, 4229–4237. https://doi.org/10.5194/acp-9-4229-2009

Keene, W. C., Stutz, J., Pszenny, A. A. P., Maben, J. R., Fischer, E. V., Smith, A. M., et al. (2007). Inorganic chlorine and bromine in coastal New England air during summer. *Journal of Geophysical Research*, *112*, D10S12. https://doi.org/10.1029/2006JD007689

Kim, S., Wolfe, G. M., Mauldin, L., Cantrell, C., Guenther, A., Karl, T., et al. (2013). Evaluation of HO_x sources and cycling using measurement-constrained model calculations in a 2-methyl-3-butene-2-ol (MBO) and monoterpene (MT) dominated ecosystem. *Atmospheric Chemistry and Physics*, *13*, 2031–2044. https://doi.org/10.5194/acp-13-2031-2013

Knipping, E. M., & Dabdub, D. (2002). Modeling Cl2 formation from aqueous NaCl particles: Evidence for interfacial reactions and importance of Cl2 decomposition in alkaline solution. *Journal of Geophysical Research: Atmospheres*, *107*(D18), 4360. https://doi.org/10.1029/2001JD000867

Knipping, E. M., Lakin, M. J., Foster, K. L., Jungwirth, P., Tobias, D. J., Gerber, R. B., et al. (2000). Experiments and simulations of ion-enhanced interfacial chemistry on aqueous NaCl aerosols. *Science*, *288*(5464), 301–306. https://doi.org/10.1126/science.288.5464.301

Laskin, A., Wang, H., Robertson, W. H., Cowin, J. P., Ezell, M. J., & Finlayson-Pitts, B. J. (2006). A new approach to determining gas-particle reaction probabilities and application to the heterogeneous reaction of deliquesced sodium chloride particles with gas-phase hydroxyl radicals. *The Journal of Physical Chemistry A*, *110*(36), 10619–10627. https://doi.org/10.1021/jp063263+

Lawler, M. J., Finley, B. D., Keene, W. C., Pszenny, A. A. P., Read, K. A., Von Glasow, R., & Saltzman, E. S. (2009). Pollution-enhanced reactive chlorine chemistry in the eastern tropical Atlantic boundary layer. *Geophysical Research Letters*, *36*, L08810. https://doi.org/10.1029/2008GL036666

Lawler, M. J., Sander, R., Carpenter, L. J., Lee, J. D., von Glasow, R., Sommariva, R., & Saltzman, E. S. (2011). HOCl and Cl_2 observations in marine air. *Atmospheric Chemistry and Physics*, *11*, 7617–7628. https://doi.org/10.5194/acp-11-7617-2011

Le Breton, M., Hallquist, Å. M., Pathak, R. K., Simpson, D., Wang, Y., Johansson, J., et al. (2018). Chlorine oxidation of VOCs at a semi-rural site in Beijing: significant chlorine liberation from $ClNO_2$ and subsequent gas- and particle-phase Cl–VOC production. *Atmospheric Chemistry and Physics*, *18*, 13013–13030. https://doi.org/10.5194/acp-18-13013-2018

Lee, J. D., McFiggans, G., Allan, J. D., Baker, A. R., Ball, S. M., Benton, A. K., et al. (2010). Reactive halogens in the marine boundary layer (RHaMBLe): The tropical North Atlantic experiments. *Atmospheric Chemistry and Physics*, *10*(3), 1031–1055. https://doi.org/10.5194/acp-10-1031-2010

Lee, Y., Huey, L. G., Wang, Y., Qu, H., Zhang, R., Ji, Y., et al. (2021). Photochemistry of volatile organic compounds in the Yellow River Delta, China: Formation of O3 and Peroxyacyl nitrates. *Journal of Geophysical Research: Atmospheres*, *126*, e2021JD035296. https://doi.org/10.1029/2021JD035296

Levine, J. G., Wolff, E. W., Jones, A. E., & Sime, L. C. (2011). The role of atomic chlorine in glacial-interglacial changes in the carbon-13 content of atmospheric methane. *Geophysical Research Letters*, *38*, L04801. https://doi.org/10.1029/2010GL046122

Liao, J., Huey, L. G., Liu, Z., Tanner, D. J., Cantrell, C. A., Orlando, J. J., et al. (2014). High levels of molecular chlorine in the Arctic atmosphere. *Nature Geoscience*, *7*, 91–94. https://doi.org/10.1038/ngeo2046

Li, Y., Nie, W., Liu, Y., Huang, D., Xu, Z., Peng, X., et al. (2020). Photoinduced production of chlorine molecules from titanium dioxide surfaces containing chloride. *Environmental Science and Technology Letters*, *7*(2), 70–75. https://doi.org/10.1021/acs.estlett.9b00704

Lim, M., Chiang, K., & Amal, R. (2006). Photochemical synthesis of chlorine gas from iron(III) and chloride solution. *Journal of Photochemistry and Photobiology A: Chemistry*, *183*, 126–132. https://doi.org/10.1016/j.jphotochem.2006.03.005

Liu, X., Qu, H., Huey, L. G., Wang, Y., Sjostedt, S., Zeng, L., et al. (2017). High levels of daytime molecular chlorine and nitryl chloride at a rural site on the North China Plain. *Environmental Science & Technology*, *51*(17), 9588–9595. https://doi.org/10.1021/acs.est.7b03039

Liu, Y., Fan, Q., Chen, X., Zhao, J., Ling, Z., Hong, Y., et al. (2018). Modeling the impact of chlorine emissions from coal combustion and prescribed waste incineration on tropospheric ozone formation in China. *Atmospheric Chemistry and Physics*, *18*(4), 2709–2724. https://doi.org/10.5194/acp-18-2709-2018

Lu, K., Guo, S., Tan, Z., Wang, H., Shang, D., Liu, Y., et al. (2019). Exploring atmospheric free-radical chemistry in China: The self-cleansing capacity and the formation of secondary air pollution. *National Science Review*, *6*(3), 579–594. https://doi.org/10.1093/nsr/nwy073

Luo, C., Mahowald, N., Bond, T., Chuang, P. Y., Artaxo, P., Siefert, R., et al. (2008). Combustion iron distribution and deposition. *Global Biogeochemical Cycles*, *22*, GB1012. https://doi.org/10.1029/2007GB002964

McNamara, S. M., Raso, A. R., Wang, S., Thanekar, S., Boone, E. J., Kolesar, K. R., et al. (2019). Springtime nitrogen oxide-influenced chlorine chemistry in the coastal Arctic. *Environmental Science & Technology*, *53*, 8057–8067. https://doi.org/10.1021/acs.est.9b01797

Moffet, R. C., Furutani, H., Rödel, T. C., Henn, T. R., Sprau, P. O., Laskin, A., et al. (2012). Iron speciation and mixing in single aerosol particles from the Asian continental outflow. *Journal of Geophysical Research: Atmospheres*, *117*, D07204. https://doi.org/10.1029/2011JD016746

Nadtochenko, V. A., & Kiwi, J. (1998). Photolysis of FeOH2+ and FeCl2+ in aqueous solution. Photodissociation kinetics and quantum yields. *Inorganic Chemistry*, *37*(20), 5233–5238. https://doi.org/10.1021/ic9804723

Osthoff, H. D., Roberts, J. M., Ravishankara, A. R., Williams, E. J., Lerner, B. M., Sommariva, R., et al. (2008). High levels of nitryl chloride in the polluted subtropical marine boundary layer. *Nature Geoscience*, *1*(5), 324–328. https://doi.org/10.1038/ngeo177

Oum, K. W., Lakin, M. J., DeHaan, D. O., Brauers, T., & Finlayson–Pitts, B. J. (1998). Formation of molecular chlorine from the photolysis of ozone and aqueous sea–salt particles. *Science*, *279*, 74–76. https://doi.org/10.1126/science.279.5347.74

Pechtl, S., & von Glasow, R. (2007). Reactive chlorine in the marine boundary layer in the outflow of polluted continental air: A model study. *Geophysical Research Letters*, *34*(11). https://doi.org/10.1029/2007GL029761

Peng, X., Wang, T., Wang, W., Ravishankara, A. R., George, C., Xia, M., et al. (2021). Unraveling the daytime source of molecular chlorine in the extra-polar atmosphere. *Earth and Space Science Open Archive*. https://doi.org/10.1002/essoar.10507686.1

Peng, X., Wang, W., Xia, M., Chen, H., Ravishankara, A. R., Li, Q., et al. (2021). An unexpected large continental source of reactive bromine and chlorine with significant impact on wintertime air quality. *National Science Review*, *8*(7), nwaa304. https://doi.org/10.1093/nsr/nwaa304

Pratte, P., & Rossi, M. J. (2006). The heterogeneous kinetics of HOBr and HOCl on acidified sea salt and model aerosol at 40–90% relative humidity and ambient temperature. *Physical Chemistry Chemical Physics*, *8*(34), 3988–4001. https://doi.org/10.1039/b604321f

Priestley, M., Le Breton, M., Bannan, T. J., Worrall, S. D., Bacak, A., Smedley, A. R. D., et al. (2018). Observations of organic and inorganic chlorinated compounds and their contribution to chlorine radical concentrations in an urban environment in northern Europe during the wintertime. *Atmospheric Chemistry and Physics*, *18*, 13481–13493. https://doi.org/10.5194/acp-18-13481-2018

Pszenny, A. A. P., Keene, W. C., Jacob, D. J., Fan, S., Maben, J. R., Zetwo, M. P., et al. (1993). Evidence of inorganic chlorine gases other than hydrogen chloride in marine surface air. *Geophysical Research Letters*, *20*(8), 699–702. https://doi.org/10.1029/93GL00047

Pszenny, A. A. P., Moldanová, J., Keene, W. C., Sander, R., Maben, J. R., Martinez, M., et al. (2004). Halogen cycling and aerosol pH in the Hawaiian marine boundary layer. *Atmospheric Chemistry and Physics*, *4*(1), 147–168. https://doi.org/10.5194/acp-4-147-2004

Qiu, X., Ying, Q., Wang, S., Duan, L., Wang, Y., Lu, K., et al. (2019). Significant impact of heterogeneous reactions of reactive chlorine species on summertime atmospheric ozone and free-radical formation in North China. *The Science of the Total Environment*, *693*, 133580. https://doi.org/10.1016/j.scitotenv.2019.133580

Riedel, T. P., Bertram, T. H., Crisp, T. A., Williams, E. J., Lerner, B. M., Vlasenko, A., et al. (2012). Nitryl chloride and molecular chlorine in the coastal marine boundary layer. *Environmental Science & Technology*, *46*, 10463–10470. https://doi.org/10.1021/es204632r

Riedel, T. P., Wagner, N. L., Dubé, W. P., Middlebrook, A. M., Young, C. J., Öztürk, F., et al. (2013). Chlorine activation within urban or power plant plumes: Vertically resolved ClNO2 and Cl2 measurements from a tall tower in a polluted continental setting. *Journal of Geophysical Research: Atmospheres*, *118*(15), 8702–8715. https://doi.org/10.1002/jgrd.50637

Riva, M., Healy, R. M., Flaud, P. M., Perraudin, E., Wenger, J. C., & Villenave, E. (2015). Gas- and particle-phase products from the chlorine-initiated oxidation of polycyclic aromatic hydrocarbons. *The Journal of Physical Chemistry A*, *119*, 11170–11181. https://doi.org/10.1021/acs.jpca.5b04610

Roberts, J. M., Osthoff, H. D., Brown, S. S., & Ravishankara, A. R. (2008). N2O5 oxidizes chloride to Cl2 in acidic atmospheric aerosol. *Science*, *321*, 1059. https://doi.org/10.1126/science.1158777

Sadanaga, Y., Hirokawa, J., & Akimoto, H. (2001). Formation of molecular chlorine in dark condition: Heterogeneous reaction of ozone with sea salt in the presence of ferric ion. *Geophysical Research Letters*, *28*, 4433–4436. https://doi.org/10.1029/2001GL013722

Sander, R. (2015). Compilation of Henry's law constants (version 4.0) for water as solvent. *Atmospheric Chemistry and Physics*, *15*(8), 4399–4981. https://doi.org/10.5194/acp-15-4399-2015

Saueressig, G., Bergamaschi, P., Crowley, J., Fischer, H., & Harris, G. (1995). Carbon kinetic isotope effect in the reaction of CH4 with Cl atoms. *Geophysical Research Letters*, *22*, 1225–1228. https://doi.org/10.1029/95GL00881

Simpson, W. R., Brown, S. S., Saiz-Lopez, A., Thornton, J. A., & Glasow, R. (2015). Tropospheric halogen chemistry: Sources, cycling, and impacts. *Chemical Reviews*, *115*, 4035–4062. https://doi.org/10.1021/cr5006638

Spicer, C. W., Chapman, E. G., Finlayson-Pitts, B. J., Plastridge, R. A., Hubbe, J. M., Fast, J. D., & Berkowitz, C. M. (1998). Unexpectedly high concentrations of molecular chlorine in coastal air. *Nature*, *394*(6691), 353–356. https://doi.org/10.1038/28584

Strode, S. A., Wang, J. S., Manyin, M., Duncan, B., Hossaini, R., Keller, C. A., et al. (2020). Strong sensitivity of the isotopic composition of methane to the plausible range of tropospheric chlorine. *Atmospheric Chemistry and Physics*, *20*, 8405–8419. https://doi.org/10.5194/acp-20-8405-2020

Tanaka, P. L., Oldfield, S., Neece, J. D., Mullins, C. B., & Allen, D. T. (2000). Anthropogenic sources of chlorine and ozone formation in urban atmospheres. *Environmental Science & Technology*, *34*(21), 4470–4473. https://doi.org/10.1021/es991380v

Thornton, J. A., Kercher, J. P., Riedel, T. P., Wagner, N. L., Cozic, J., Holloway, J. S., et al. (2010). A large atomic chlorine source inferred from mid-continental reactive nitrogen chemistry. *Nature*, *464*(7286), 271–274. https://doi.org/10.1038/nature08905

Tilgner, A., & Herrmann, H. (2018). Tropospheric aqueous-phase OH oxidation chemistry: Current understanding, uptake of highly oxidized organics and its effects. In S. W. Hunt, A. Laskin, & S. A. Nizkorodov (Eds.), *Multiphase environmental chemistry in the atmosphere* (pp. 49–85). American Chemical Society.

Vogt, R., Crutzen, P., & Sander, R. (1996). A mechanism for halogen release from sea-salt aerosol in the remote marine boundary layer. *Nature*, *383*, 327–330. https://doi.org/10.1038/383327a0

Wang, D. S., & Ruiz, L. H. (2017). Secondary organic aerosol from chlorine-initiated oxidation of isoprene. *Atmospheric Chemistry and Physics*, *17*, 13491–13508. https://doi.org/10.5194/acp-17-13491-2017

Wang, J., Li, S., Li, H., Qian, X., Li, X., Liu, X., et al. (2017). Trace metals and magnetic particles in PM 2.5: Magnetic identification and its implications. *Scientific Reports*, *7*(1), 1–11. https://doi.org/10.1038/s41598-017-08628-0

Wang, S., & Pratt, K. A. (2017). Molecular halogens above the Arctic snowpack: Emissions, diurnal variations, and recycling mechanisms. *Journal of Geophysical Research: Atmospheres*, *122*(21), 11991–12007. https://doi.org/10.1002/2017JD027175

Wang, X., Jacob, D. J., Eastham, S. D., Sulprizio, M. P., Zhu, L., Chen, Q., et al. (2019). The role of chlorine in global tropospheric chemistry. *Atmospheric Chemistry and Physics*, *19*(6), 3981–4003. https://doi.org/10.5194/acp-19-3981-2019

Wittmer, J., Bleicher, S., Ofner, J., & Zetzsch, C. (2015). Iron(III)-induced activation of chloride from artificial sea-salt aerosol. *Environmental Chemistry*, *12*, 461–475. https://doi.org/10.1071/EN14279

Wittmer, J., Bleicher, S., & Zetzsch, C. (2015). Iron(III)-induced activation of chloride and bromide from modeled salt pans. *The Journal of Physical Chemistry A*, *119*(19), 4373–4385. https://doi.org/10.1021/jp508006s

Wolfe, G. M., Cantrell, C., Kim, S., Mauldin, R. L., III, Karl, T., Harley, P., et al. (2014). Missing peroxy radical sources within a summertime ponderosa pine forest. *Atmospheric Chemistry and Physics*, *14*(9), 4715–4732. https://doi.org/10.5194/acp-14-4715-2014

Wolfe, G. M., Marvin, M. R., Roberts, S. J., Travis, K. R., & Liao, J. (2016). The Framework for 0-D atmospheric modeling (F0AM) v3.1. *Geoscientific Model Development*, *9*(9), 3309–3319. https://doi.org/10.5194/gmd-9-3309-2016

Wu, R., Zhao, Y., Zhang, J., & Zhang, L. (2020). Variability and sources of ambient volatile organic compounds based on online measurements in a suburban region of Nanjing, Eastern China. *Aerosol and Air Quality Research*, *20*(3), 606–619. https://doi.org/10.4209/aaqr.2019.10.0517

Xia, M., Peng, X., Wang, W., Yu, C., Sun, P., Li, Y., et al. (2020). Significant production of ClNO2 and possible source of Cl2 from N2O5 uptake at a suburban site in eastern China. *Atmospheric Chemistry and Physics*, *20*(10), 6147–6158. https://doi.org/10.5194/acp-20-6147-2020

Xu, Z. N., Nie, W., Liu, Y. L., Sun, P., Huang, D. D., Yan, C., et al. (2021). Multifunctional products of isoprene oxidation in polluted atmosphere and their contribution to SOA. *Geophysical Research Letters*, *48*, e2020GL089276. https://doi.org/10.1029/2020GL089276

Xue, L. K., Saunders, S. M., Wang, T., Gao, R., Wang, X. F., Zhang, Q. Z., & Wang, W. X. (2015). Development of a chlorine chemistry module for the master chemical mechanism. *Geoscientific Model Development*, *8*, 3151–3162. https://doi.org/10.5194/gmd-8-3151-2015

Yi, X., Yin, S., Huang, L., Li, H., Wang, Y., Wang, Q., et al. (2021). Anthropogenic emissions of atomic chlorine precursors in the Yangtze River Delta region, China. *Science of the Total Environment*, *771*, 144644. https://doi.org/10.1016/j.scitotenv.2020.144644

Zhou, Y., Zhao, Y., Mao, P., Zhang, Q., Zhang, J., Qiu, L., & Yang, Y. (2017). Development of a high-resolution emission inventory and its evaluation and application through air quality modeling for Jiangsu Province, China. *Atmospheric Chemistry and Physics*, *17*, 211–233. https://doi.org/10.5194/acp-17-211-2017

Zhu, Y., Li, W., Lin, Q., Yuan, Q., Liu, L., Zhang, J., et al. (2020). Iron solubility in fine particles associated with secondary acidic aerosols in east China. *Environmental Pollution*, *264*, 114769. https://doi.org/10.1016/j.envpol.2020.114769

References From the Supporting Information

Burkholder, J. B., Sander, S. P., Abbatt, J. P. D., Barker, J. R., Huie, R. E., Kolb, C. E., et al. (2015). *Chemical kinetics and photochemical data for use in atmospheric studies: Evaluation number 18*. Jet Propulsion Laboratory, National Aeronautics and Space Administration.

Ehhalt, D. H., & Rohrer, F. (2009). The tropospheric cycle of H2: A critical review. *Tellus B: Chemical and Physical Meteorology*, *61*(3), 500–535. https://doi.org/10.1111/j.1600-0889.2009.00416.x

Sander, S. P., Friedl, R. R., Abbatt, J. P. D., Barker, J. R., Burkholder, J. B., Golden, et al. (2011). *Chemical kinetics and photochemical data for use in atmospheric studies: Evaluation number 17*. Jet Propulsion Laboratory, National Aeronautics and Space Administration.